# Analysis of Symbol-Design Strategies for Intrapulse Radar-Embedded Communications

**JUSTIN G. METCALF,** Member, IEEE
University of Kansas
Lawrence, KS, USA
and
Air Force Research Laboratory
Wright-Patterson Air Force Base, OH, USA

**CENK SAHIN,** Graduate Student Member, IEEE
**SHANNON D. BLUNT,** Senior Member, IEEE
University of Kansas
Lawrence, KS, USA

**MURALIDHAR RANGASWAMY,** Fellow, IEEE
Air Force Research Laboratory
Wright-Patterson Air Force Base, OH, USA

**The design of communication symbols that may be embedded on an intrapulse basis into the backscatter generated by a high-power, pulsed radar is considered. This framework requires the asynchronous detection of transmitted symbols in a high-interference environment that degrades the capabilities of conventional intercept receivers. The impact of symbol design and filter structure upon the successful detection of covert symbols by the intended receiver and a hypothetical partially clairvoyant intercept receiver is examined.**

Manuscript received September 10, 2014; revised February 18, 2015, April 29, 2015; released for publication April 29, 2015.

DOI. No. 10.1109/TAES.2015.140675.

Refereeing of this contribution was handled by L. Kaplan.

This work was supported by the Air Force Office of Scientific Research under contract FA9550-12-1-0220.

Authors' addresses: J. G. Metcalf, M. Rangaswamy, Air Force Research Laboratory, Sensors Directorate, 2241 Avionics Circle, Wright-Patterson Air Force Base, OH 45433, E-mail: (justin.metcalf@us.af.mil); C. Sahin, S. D. Blunt, University of Kansas, Electrical Engineering and Computer Science, 1520 W. 15th St., Eaton Hall, Lawrence, KS 66045.



## I. INTRODUCTION

As the spectrum becomes more congested, increasing attention is being paid to multimode systems with both sensing and communications capabilities. A prime example of this form of spectral cohabitation comes from the automotive research community [1–4]. In addition, the defense community is sponsoring initiatives focused on allowing radar and communication systems to coexist in the same spectrum (e.g., the DARPA SSPARC program [5]). This work continues in the line of [6–9] to examine methods of designing and detecting low-probability-of-intercept (LPI) communication symbols that reside within radar clutter. The additional constraint of LPI requires further considerations beyond those of other multimode schemes.

In [6–9] a framework for LPI communication using masking radar clutter on an intrapulse basis was developed and analyzed. Based on observations on symbol optimization from [9], here this concept is expanded to consider enhanced symbol and filter design strategies that incorporate the spectral shape of the clutter. In addition to the metrics used to evaluate a traditional communication system (e.g., bit error rate, signal-to-interference-plus-noise ratio), an LPI system must simultaneously minimize the detection probability at prospective intercept receivers, and so this attribute is likewise examined.

A spread-spectrum system is generally defined as a communication system where the information bandwidth is less than the transmission bandwidth [10]. The communication waveform may be directly spread over a wide bandwidth or a transmission may hop rapidly over various frequencies. Spread-spectrum transmission is naturally useful in an LPI context. The diversity afforded by spreading the information over a wider bandwidth provides resistance to narrowband interference and increases the difficulty for an intercept receiver to detect the transmission [10, 11]. Here we consider a form of direct spreading that is tailored to an external interference source, namely radar clutter.

The operational concept under consideration has four primary components, as shown in Fig. 1. First, an area is illuminated with a radar waveform, here presumed to be pulsed at an arbitrary pulse repetition frequency. Second, a transponder or tag (hereafter referred to as the tag for simplicity) that wishes to transmit a covert communication symbol injects an LPI symbol among the clutter (ambient reflections) generated by the radar emission. Third, a desired receiver (or multiple receivers) is available to detect and demodulate the covert clutter-embedded symbol and recover the information conveyed by the tag. Finally, intercept receivers may exist that attempt to detect any covert transmissions.

The tag, upon being triggered by the incident radar waveform, emits a communication symbol that is characterized such that the desired receiver(s) may readily demodulate the symbol but the intercept receiver cannot

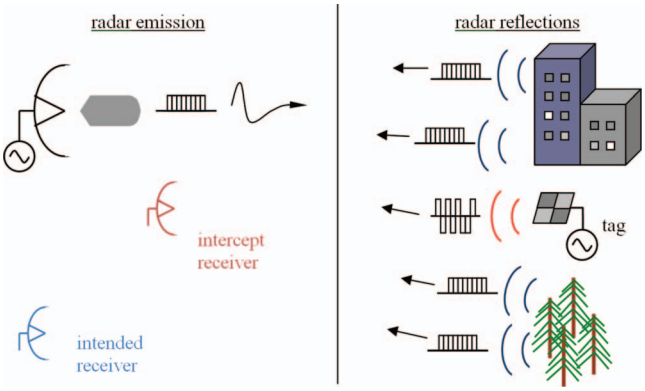


Fig. 1. Generic radar-embedded communications system.

detect its embedded presence the radar clutter. By transmitting communication symbols on a per-pulse basis, the tag realizes a data rate on the order of the pulse repetition frequency. The radar and desired receiver may be colocated or separated, with the former also enabling the tag to make use of time reversal to exploit multipath for space-time focusing [9]. Note that this covert communication framework developed in [6–9] is general and admits any number of transmitting tags, as long as the respective symbols do not completely overlap. However, for notational and analytical convenience, here we consider the case of a single transmitting tag.

It is important to note that the framework under consideration inherently imposes several practical trade-offs and constraints on symbol and receiver design. The constraints with the greatest influence are summarized in Table I; they are necessarily interrelated and driven by the dual goals of maximizing the data rate through the communication system while minimizing the probability of intercept. The presence of radar clutter offers an opportunity to construct LPI communication symbols. However, constructing communication symbols to take advantage of the masking radar clutter necessarily limits the symbol-design choices available. For example, to maintain LPI, the symbols are designed to be correlated with the waveform-induced clutter and occupy a similar temporal and spectral footprint via subspace projection. Therefore, the symbols occupy a linear space with limited degrees of freedom and must be transmitted in a burst mode triggered by the incident radar illumination, such that the repetition rate of the burst mode is constrained to the requirements of the illuminating radar rather than any characteristics desired by the communication receivers. In practice, the surrounding clutter is unknown and the radar waveform must be determined from the observed illumination, which may contain multipath and possess relative sample-timing differences between the tag and desired receiver. Therefore, as the symbols are dynamically generated based on the characteristics of the radar illumination, the symbol and receive-filter designs should be robust to mismatch between the tag and receiver. In addition, the receiver must be able to synchronize with the received symbol without the aid of pilot symbols or an external control channel. Finally, the intercept receiver must be considered. Quantifying the LPI nature of a given transmission scheme is not a well-defined problem [12]. Therefore, a hypothesized worst-case bound on intercept-receiver performance is employed here, in which the metric incorporates some clairvoyant knowledge regarding the possible embedded symbols.

The observations made in [6, 7, 9] have developed and informed the constraints in Table I. Here we use these prior observations to define and analyze alternative symbol-design structures with the goal of gaining insight into what factors impact overall performance under the given constraints. Specifically, the well-known water-filling approach is examined, along with the impact of shaping according to the spectral response of the radar illumination. The proposed symbol designs are intended not to represent the optimal symbols but instead to highlight attractive symbol attributes within the practical constraints of the radar-embedded communication problem. As the approaches presented here do not alter the fundamental subspace-projection approach of [6–9], the robustness to clutter covariance estimation mismatch is maintained. However, while the computational complexity of the approach must be considered (point 6 of Table I), the analysis of the computational complexity is beyond the scope of this work.

The remainder of the paper is organized as follows. In Section II we examine new designs for intrapulse radar-embedded symbols, using the classic direct-sequence spread spectrum (DSSS) and previous schemes from [7, 9] for comparison. Section III then briefly reviews the two-stage Neyman–Pearson (NP) receiver structure from [9]. In Section IV the proposed symbols are examined in conjunction with three filter structures, and the processing gain relative to an energy detector (i.e., total-power radiometer-based intercept receiver) is examined. Finally, Section V evaluates the probability of detection by the partially clairvoyant intercept receiver and by the desired receiver, along with bit error rate.

## II. LPI COMMUNICATION-SYMBOL DESIGN

The design of the communication symbols is constrained by the factors in Table I. Therefore, we consider a general class of symbols with desirable properties to meet the design criteria discussed in Section I. Each of these symbol-design methods has been informed by the developments of [6, 7, 9]. First, a traditional spread-spectrum symbol design is presented to provide a performance baseline that does not account for the presence of masking radar clutter. Then, to examine the impact of spectral shaping to better fit the surrounding clutter (relative to the original dominant-projection [DP] approach [7]), the spectral roll-off of the radar illumination is factored into the symbol design. In addition, the well-known water-filling scheme is examined within this

TABLE I
Practical Design Constraints for Intrapulse Radar-Embedded Communications

1. Radar, tag, and desired receiver are not synchronized.
2. Symbols must be determined independently at the tag and desired receiver based on the observed radar illumination (possible timing uncertainty and multipath differences).
3. The surrounding clutter structure is not known exactly, though it can be viewed as a random signal convolved with the radar waveform.
4. Symbols are designed to be partially correlated with the clutter but still separable from one another on receive.
5. Symbols have temporal and spectral footprint commensurate with the radar waveform.
6. Symbol design must occur in a reasonable time frame (while radar illumination persists).

clutter masking context, with a modified version proposed that also addresses the desired LPI attribute.

For the communication symbols to be LPI, they are designed to be partially correlated with the clutter yet possess a structure that may be used by the desired receiver to separate them from the clutter. Let $N$ be the number of discrete samples required to fully characterize the radar waveform based on Nyquist sampling according to the 3 dB bandwidth. Define $M$ as an oversampling factor that is used to control the amount of additional spreading the communication symbols undergo in relation to the radar 3 dB bandwidth. The continuous radar waveform is denoted $s(t)$, and its discrete oversampled representation is the length-$NM$ vector $\mathbf{s}$.

As shown in [7] and [9], the ambient signal generated by the collection of radar reflections and collected at an arbitrary receiver can be expressed as

$$\mathbf{y} = \mathbf{S}\mathbf{x} + \mathbf{u}, \tag{1}$$

where $\mathbf{u}$ is an $NM \times 1$ vector of complex additive Gaussian noise and $\mathbf{S}\mathbf{x}$ is the discrete convolution between the radar waveform and the arbitrary clutter process $\mathbf{x}$, which is unknown. This discrete convolution is performed using the $NM \times (2NM-1)$ Toeplitz $\mathbf{S}$ that consists of delay shifts of the radar waveform and is expressed as

$$\mathbf{S} = \begin{bmatrix} s_{NM-1} & s_{NM-2} & \cdots & s_0 & 0 & \cdots & 0 \\ 0 & s_{NM-1} & \cdots & s_1 & s_0 & \cdots & 0 \\ \vdots & \vdots & \ddots & \vdots & \vdots & \ddots & \vdots \\ 0 & 0 & \cdots & s_{NM-1} & s_{NM-2} & \cdots & s_0 \end{bmatrix}. \tag{2}$$

The normalized correlation of the clutter response admits the eigen decomposition [7, 9]

$$\begin{aligned} \frac{1}{\sigma_x^2} E\left[(\mathbf{S}\mathbf{x})(\mathbf{S}\mathbf{x})^{\mathrm{H}}\right] &= \frac{1}{\sigma_x^2}\mathbf{S}E\left[\mathbf{x}\mathbf{x}^{\mathrm{H}}\right]\mathbf{S}^{\mathrm{H}} \\ &= \mathbf{S}\mathbf{S}^{\mathrm{H}} \\ &= \mathbf{V}\mathbf{\Lambda}\mathbf{V}^{\mathrm{H}}, \end{aligned} \tag{3}$$

where $\mathbf{\Lambda}$ is a diagonal matrix of eigenvalues in descending order associated with the eigenvectors in $\mathbf{V}$ and the clutter process is assumed to be uncorrelated in range with equal variance at each sample. This assumption reflects the lack of knowledge regarding the correlation of surrounding clutter, and could readily be modified if such knowledge were available (e.g., if additional masking clutter were artificially generated as suggested in [7]). The methods considered in the following all operate on a subspace basis, reducing the impact of mismatch between covariance matrix estimates due to synchronization difference [7] or multipath [9].

For simplicity, we assume that the radar waveform is constant modulus and normalized such that $\mathbf{s}^{\mathrm{H}}\mathbf{s} = 1$. Therefore,

$$\begin{aligned} \mathrm{tr}\left\{\mathbf{S}\mathbf{S}^{\mathrm{H}}\right\} &= \sum_{i=1}^{NM} \mathbf{s}^{\mathrm{H}}\mathbf{s} = NM \\ &= \mathrm{tr}\left\{\mathbf{\Lambda}\right\} = \mathrm{tr}\left\{\mathbf{V}\mathbf{\Lambda}\mathbf{V}^{\mathrm{H}}\right\}, \end{aligned} \tag{4}$$

where the equality of the first and last terms is taken from (3).

### A. Direct-Sequence Spread Spectrum (DSSS)

To provide a performance baseline in which the masking clutter is not utilized, first consider a conventional communication system with a total transmit-energy constraint $\gamma$. However, instead of allocating transmitted power to, for example, subchannels within an orthogonal-frequency division multiplexing framework, here power is allocated according the eigenvectors of the overall clutter-plus-noise space induced by the radar illumination. The classical DSSS approach spreads the symbol energy uniformly over the transmit bandwidth [10]. Therefore, an eigenspace-based DSSS approach is to assign a uniform transmit power of $\gamma/NM$ to each eigenchannel (eigenvector), so that the $k$th DSSS symbol can be defined as

$$\begin{aligned} \mathbf{c}_{\mathrm{DSSS},k} &= \frac{\gamma}{NM}\mathbf{V}^{\mathrm{H}}\mathbf{b}_k \\ &= \frac{\gamma}{NM}\mathbf{q}_k. \end{aligned} \tag{5}$$

In (5), $\mathbf{b}_k$ is an $NM \times 1$ pseudorandom spreading vector known to both the tag and any desired receivers, and we have defined

$$\mathbf{q}_k \doteq \mathbf{V}^{\mathrm{H}}\mathbf{b}_k \tag{6}$$

to be the transformed spreading vector. The approach of (5) differs from traditional DSSS schemes in that the spreading vectors provide an alphabet of communication symbols rather than distinguishing between users, as is the case in a traditional code-division multiple-access scheme.

## B. Dominant Projection (DP)

One possible method to mitigate the impact of the clutter on communication performance is to allocate no transmit power to eigenchannels associated with a strong clutter response. The eigenvectors $\mathbf{V}$ in (3) can be partitioned into subspaces associated with the $m$ largest (dominant; D) and $NM - m$ smallest (nondominant; ND) eigenvalues [7, 9] as

$$\mathbf{V}\boldsymbol{\Lambda}\mathbf{V}^{\mathrm{H}} = \left[\, \mathbf{V}_{\mathrm{D}} \,\middle|\, \mathbf{V}_{\mathrm{ND}} \,\right] \left[\begin{array}{c|c} \boldsymbol{\Lambda}_{\mathrm{D}} & \mathbf{0} \\ \hline \mathbf{0} & \boldsymbol{\Lambda}_{\mathrm{ND}} \end{array}\right] \left[\begin{array}{c} \mathbf{V}_{\mathrm{D}}^{\mathrm{H}} \\ \hline \mathbf{V}_{\mathrm{ND}}^{\mathrm{H}} \end{array}\right]. \tag{7}$$

A logical division of dominant and nondominant subspaces is to designate the dominant subspace to be $m = N$ (i.e., the time-bandwidth dimensionality occupied by the radar waveform) and the nondominant subspace to be the eigenvectors associated with the remaining $NM - N$ eigenvalues [7]. However, varying the size of dominant and nondominant subspaces offers more freedom with which to design the communication symbols, thus allowing for optimization [9]. The method of symbol design in [7, 9] formed the projection matrix

$$\begin{aligned} \mathbf{A} &= \mathbf{I} - \mathbf{V}_{\mathrm{D},m}\mathbf{V}_{\mathrm{D},m}^{\mathrm{H}} \\ &= \mathbf{V}_{\mathrm{ND},m}\mathbf{V}_{\mathrm{ND},m}^{\mathrm{H}}, \end{aligned} \tag{8}$$

where the subscript $m$ indicates the number of dominant eigenvectors in $\mathbf{V}_{\mathrm{D},m}$. The $k$th DP communication symbol is then formed as

$$\begin{aligned} \mathbf{c}_{\mathrm{DP},k} &= \beta_{\mathrm{DP},m}^{1/2}\mathbf{A}\mathbf{b}_k \\ &= \beta_{\mathrm{DP},m}^{1/2}\mathbf{V}_{\mathrm{ND},m}\mathbf{V}_{\mathrm{ND},m}^{\mathrm{H}}\mathbf{b}_k \\ &= \beta_{\mathrm{DP},m}^{1/2}\mathbf{V}_{\mathrm{ND},m}\mathbf{q}_{\mathrm{ND},k}, \end{aligned} \tag{9}$$

where $\beta_{\mathrm{DP},m}^{1/2}$ is a scaling factor introduced here to enable a fair comparison between the different symbol design strategies, and $\mathbf{q}_{\mathrm{ND},k} = \mathbf{V}_{\mathrm{ND},m}^{\mathrm{H}}\mathbf{b}_k$ is the $(NM - m) \times 1$ transformed spreading vector associated with the nondominant subspace. For $\|\mathbf{b}_k\|^2 = 1$ and $\mathbf{b}_k$ an $NM \times 1$ vector, we find [9]

$$\begin{aligned} \left|b_{k,i}\right|_{\mathrm{avg}}^2 &= \left|q_{k,i}\right|_{\mathrm{avg}}^2 \\ &\approx \frac{1}{NM}, \end{aligned} \tag{10}$$

since $\mathbf{V}$ is a unitary transform.

The expected transmitted signal power of (9) is

$$\begin{aligned} S &= \left\|\mathbf{c}_{\mathrm{DP},k}\right\|^2 = \mathbf{c}_{\mathrm{DP},k}^{\mathrm{H}}\mathbf{c}_{\mathrm{DP},k} \\ &= \left(\beta_{\mathrm{DP},m}^{1/2}\mathbf{q}_{\mathrm{ND},k}^{\mathrm{H}}\mathbf{V}_{\mathrm{ND},m}^{\mathrm{H}}\right)\left(\beta_{\mathrm{DP},m}^{1/2}\mathbf{V}_{\mathrm{ND},m}\mathbf{q}_{\mathrm{ND},k}\right) \\ &= \beta_{\mathrm{DP},m}\mathbf{q}_{\mathrm{ND},k}^{\mathrm{H}}\mathbf{q}_{\mathrm{ND},k} \\ &\approx \beta_{\mathrm{DP},m}\sum_{i=m+1}^{NM}\left|q_{k,i}\right|_{\mathrm{avg}}^2 \\ &= \frac{\beta_{\mathrm{DP},m}(NM - m)}{NM}. \end{aligned} \tag{11}$$

To allow for a constant transmit energy of $\gamma$ regardless of the dimensionality $m$ of the dominant subspace, examination of (11) yields a scaling factor of

$$\beta_{\mathrm{DP},m} = \frac{\gamma NM}{NM - m}. \tag{12}$$

The DP method of [7, 9] takes advantage of the clutter response structure imposed by the radar waveform to shape communication symbols that are correlated with, yet separable from, the clutter, assuming knowledge of $\mathbf{b}_k$. In addition, through the use of the nondominant subspace as a whole (as opposed to individual nondominant eigenvectors), the symbols generated by the DP method are relatively unchanged even when the observed radar waveform is sampled with a relative timing offset between the tag and desired receiver or is corrupted by multipath [7, 9]. Notice that at the extreme case of $m = 0$, due to the orthonormal nature of eigenvectors the DP method becomes analogous to the classical DSSS method of Section II-A. However, the information contained within the eigenvalues $\boldsymbol{\Lambda}$ is ignored with the DP approach. In contrast, we now consider the impact of incorporating the eigenvalues $\boldsymbol{\Lambda}$ to further shape the LPI symbols according to the clutter spectral response.

## C. Shaped Dominant Projection (SDP)

The DP symbols of (9) allocate power evenly over the entire nondominant subspace, which, as shown in [9], impacts the optimal dimensionality to ensure that LPI is maintained. The eigenvalues of (3) provide information on the relative clutter-plus-noise power at each eigenchannel. In particular, the spectral shape of the clutter-plus-noise response exhibits a roll-off between the 3 dB bandwidth of the radar waveform and the noise floor. Through incorporation of knowledge of the eigenvalues into the symbol design, the spectrum occupied by the communication symbols can more closely imitate the spectral shape of the roll-off and thereby improve LPI performance.

Define the $k$th SDP symbol as

$$\begin{aligned} \mathbf{c}_{\mathrm{SDP},k} &= \beta_{\mathrm{SDP}}^{1/2}\mathbf{V}_{\mathrm{ND},m}\boldsymbol{\Lambda}_{\mathrm{ND},m}^{1/2}\mathbf{V}_{\mathrm{ND},m}^{\mathrm{H}}\mathbf{b}_k \\ &= \beta_{\mathrm{SDP}}^{1/2}\mathbf{V}_{\mathrm{ND},m}\boldsymbol{\Lambda}_{\mathrm{ND},m}^{1/2}\mathbf{q}_{\mathrm{ND},k}, \end{aligned} \tag{13}$$

with scaling factor

$$\beta_{\mathrm{SDP}} = \frac{\gamma NM}{\mathrm{tr}\left\{\boldsymbol{\Lambda}_{\mathrm{ND},m}\right\}}, \tag{14}$$

to ensure that the overall symbol energy is $\gamma$. Compared to the DP symbol in (9), the SDP symbol in (13) includes the $\Lambda_{\mathrm{ND}}$ term that serves to shape the symbol spectrum to match that of the radar clutter (in the roll-off region, since only the nondominant portion is addressed).

## D. Shaped Water Filling

A well-known method to shape the power across a set of channels is to assign power according to the inverse of the associated gains or losses (known as water filling

[13]). Applying this principle to the present symbol-design problem would mean that eigenvectors associated with the strongest clutter response would be transmitted at the lowest power and vice versa. Thus, a $k$th water-filling (WF) symbol could be defined as

$$\begin{aligned}\mathbf{c}_{\mathrm{WF},k} &= \beta_{\mathrm{WF}}^{1/2}\mathbf{V}\boldsymbol{\Lambda}^{-1/2}\mathbf{V}^{\mathrm{H}}\mathbf{b}_k \\ &= \beta_{\mathrm{WF}}^{1/2}\mathbf{V}\boldsymbol{\Lambda}^{-1/2}\mathbf{q}_k,\end{aligned} \tag{15}$$

where $\beta_{\mathrm{WF}}$ is the normalizing scale factor

$$\beta_{\mathrm{WF}} = \frac{\gamma NM}{\mathrm{tr}\left\{\boldsymbol{\Lambda}^{-1}\right\}}. \tag{16}$$

For the WF approach, the eigenchannels with the greatest allocated power will coincide with the lowest clutter-plus-noise channel response. However, through transmission of the greatest power on the eigenchannel with the lowest interference, the LPI performance would clearly suffer. Therefore, consider a partitioned approach that combines WF with the previous symbol shaping. Define the partitioned eigenvalue matrix for this hybrid shaped water-filling (SWF) formulation as

$$\boldsymbol{\Lambda}_{\mathrm{P},m} = \left[\begin{array}{c|c} \boldsymbol{\Lambda}_{\mathrm{D},m}^{-1} & \mathbf{0} \\ \hline \mathbf{0} & \boldsymbol{\Lambda}_{\mathrm{ND},m} \end{array}\right], \tag{17}$$

where the dimensionality $m$ still provides an optimizable parameter as in [9]. The $k$th SWF communication symbol is thus

$$\begin{aligned}\mathbf{c}_{\mathrm{SWF},k} &= \beta_{\mathrm{SWF}}^{1/2}\mathbf{V}\boldsymbol{\Lambda}_{\mathrm{P},m}^{1/2}\mathbf{V}\boldsymbol{\Lambda}^{-1/2}\mathbf{q}_k \\ &= \beta_{\mathrm{SWF}}^{1/2}\mathbf{V}\boldsymbol{\Lambda}_{\mathrm{P},m}^{1/2}\mathbf{q}_k,\end{aligned} \tag{18}$$

where

$$\beta_{\mathrm{SWF}} = \frac{\gamma NM}{\mathrm{tr}\left\{\boldsymbol{\Lambda}_{\mathrm{P},m}\right\}}. \tag{19}$$

Note that at the extreme of $m = NM$, the SWF symbol design subsumes the WF symbol design. Therefore, from this point forward we consider only the more general SWF approach.

Taking inspiration from the classical WF approach to maximizing capacity under a power constraint [13], one could discard the eigenchannels associated with the greatest clutter response. Such an approach naturally leads to the SDP method, defined in (13). Therefore, the SDP and SWF symbol designs represent classes of symbols that should provide insight into preferable structures based on the many practical implementation constraints.

## E. Spectral Content of LPI Symbols

Spectrally, the environment contains contributions from the clutter as well as ambient thermal noise. Assuming the clutter power is much greater than the noise power, the clutter subspace can be defined as the subspace spanned by the first $N$ eigenvectors (i.e., the time-bandwidth product of the radar waveform). The noise subspace is then spanned by the remaining $NM - N$ eigenvectors. As the dominant and nondominant subspaces have been defined generally, with boundary

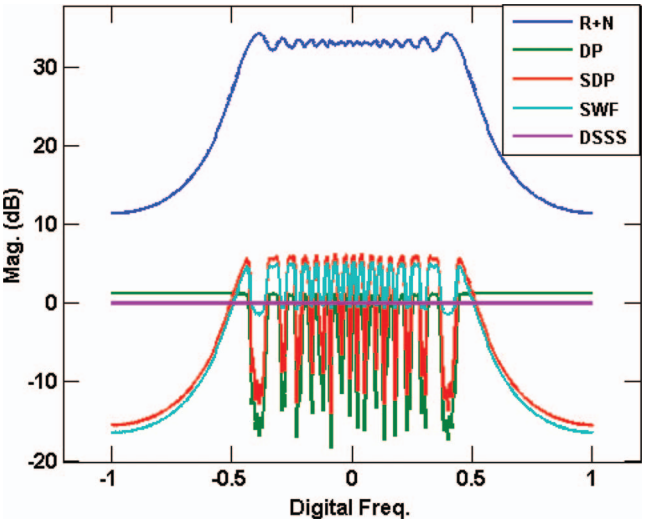


Fig. 2. Spectral content for radar-embedded communication symbols, $m = 32$.

given by $m$, the resultant communication symbols have different forms depending on the formation of the projection matrices with relation to the noise and clutter subspaces. Here we illustrate this dependence for several choices of $m$ by showing the average spectral content of the various symbol-design methods. This examination is meant to provide an intuition about the response of each symbol-design method and further justification for each method used.

In all cases, $10^6$ communication symbols were formed from random-phase spreading vectors. The spectral content of these symbols were determined and averaged. The radar waveform is a linearly frequency-modulated waveform [14] with a time-bandwidth product of $N = 64$, oversampled by a factor of $M = 2$. We use the DSSS method as a baseline, and additionally show the average clutter-plus-noise response (denoted as R + N) with a clutter-to-noise ratio (CNR) of 30 dB. All communication symbols are constrained to have a constant power constraint of $\gamma = 1$, providing a 0 dB signal-to-noise ratio (SNR).

First, Fig. 2 illustrates the average spectral content when the dominant subspace is set to be half of the waveform time-bandwidth product. For the parameters given, this condition occurs when $m = 32$. The DP method results in nulls at the dominant eigenchannels (which coincide with the peaks in the clutter response), but to maintain the constant transmit power the nondominant eigenchannels are transmitted at a higher power than the DSSS symbols (which has a uniform transmit power over all eigenchannels). This scaling causes the DP method to have the largest transmit power in the noise subspace out of all the symbol-design methods under consideration. In contrast, the SDP symbols display a roll-off in the eigenchannels associated with the transition from clutter to noise subspace that mirrors the clutter-plus-noise spectrum. Also, the SDP symbols place shallower nulls at

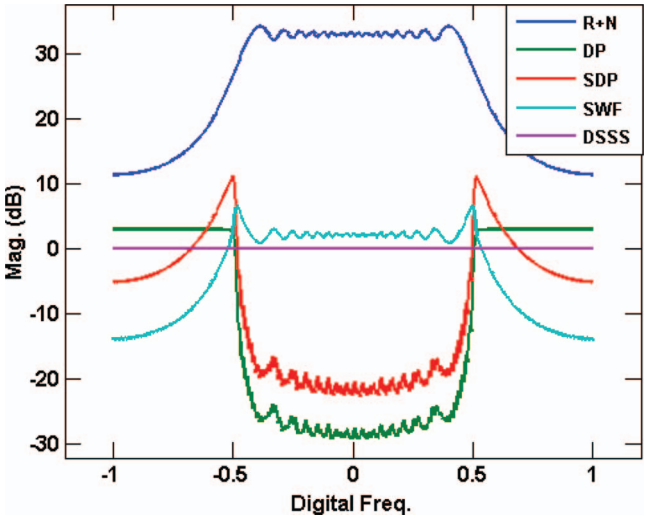


Fig. 3. Spectral content for radar-embedded communication symbols, $m = 64$.

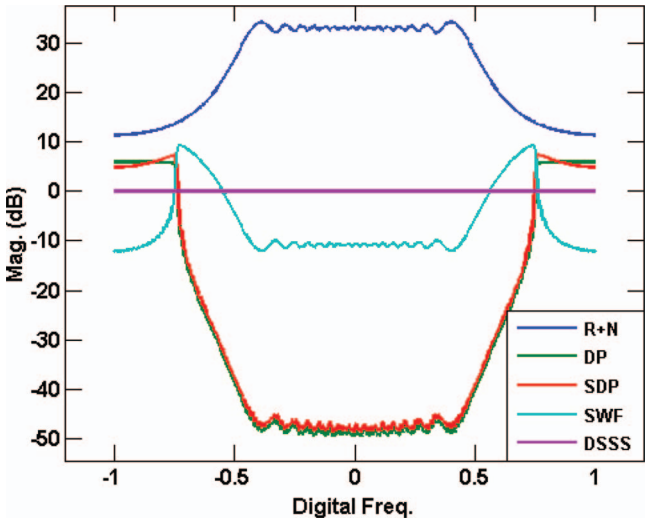


Fig. 4. Spectral content for radar-embedded communication symbols, $m = 96$.

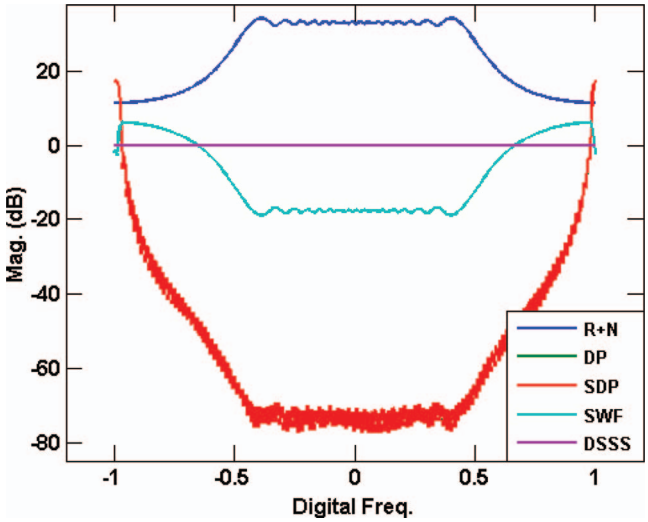


Fig. 5. Spectral content for radar-embedded communication symbols, $m = 126$. SWF now closely approximates standard WF.

the dominant eigenchannels and assign additional power (relative to the DP method) to the eigenchannels that are in the clutter subspace but are considered (through the value of $m$) to be in the nondominant subspace. Finally, the SWF symbols produce a spectrum between the extremes of the DP and SDP methods. As the dominant eigenchannels are weighted by the inverse of their eigenvalues, rather than projected out, the spectral response is shallowly suppressed rather than nulled. Therefore, slightly more power is transmitted in the clutter subspace by the SWF symbols than the SDP symbols.

Next, Fig. 3 depicts the case where $m = N = 64$. In other words, the clutter subspace is considered to be the dominant subspace and the noise subspace is the nondominant subspace (for $M = 2$). Once more, the SWF symbols produce a lower response in the noise subspace than either the DP or SDP method and allocates the most power of all symbol-design methods to the clutter subspace. However, the SDP method allows the symbol to allocate power where there is spectral bleeding between the clutter and noise subspaces, which results in more power allocated to the clutter subspace and less power at the extremes of the noise subspace relative to the DP method.

Next, Fig. 4 shows the spectral response when $m = 96$, or when the nondominant subspace is set to be equal to half of the noise subspace (the half associated with the $[NM - N]/2$ lowest eigenvalues). Notice that the relative equality of the eigenvalues and the scaling factors causes the DP and SDP methods to occupy similar regions of the spectrum. However, for the SWF symbols the inversion of the dominant eigenvalues in (17) causes a large spectral response when noise eigenvalues are considered to be part of the dominant subspace. This inversion causes a peak response $\approx$2 dB greater than the peak response of the SDP symbols for the same value of $m$. That said, while the peak value of the SWF symbol is greater than that of the DP or SDP symbols, the extreme of the noise subspace is allocated $\approx$16 dB less transmit power than for the DP or SDP symbols.

Finally, Fig. 5 examines the spectral response of the symbols when the dominant subspace is set to $m = 126$, leaving two eigenvectors for the nondominant subspace. The SDP and DP spectral responses are now approximately equivalent. In addition, the constant power constraint results in all of the power for the DP and SDP symbols being allocated to the subspace associated with the two smallest eigenvalues. Therefore, the transmitted symbol power is observed to spike in the region of the spectrum with the least masking clutter. While advantageous from an interference-avoidance perspective, these symbols are clearly not LPI. Notice the contrast between the nulling of the dominant subspace by the DP and SDP techniques and the inverse approach used by the SWF approach. This contrast was observed in Fig. 4 but is

even more apparent in Fig. 5. Weighting the dominant subspace with the associated inverse eigenvalues results in a greater amount of transmit energy being allocated to the clutter subspace than the DP and SDP methods allow. This energy allocation of SWF prevents the high power spike associated with the DP and SDP symbols. However, comparing to Fig. 4, the SWF symbols allocate an increasing amount of energy to the tails of the spectral roll-off. Therefore, as SWF approaches the traditional WF approach, the power levels associated with the noise subspace are all greater than the power levels used by the DSSS symbol design. Therefore, the increased energy associated with frequencies away from the masking clutter causes the symbol to become more vulnerable to interception by intercept-receiver methods based on energy detection [11].

## III. SYMBOL DETECTION

Once the symbol has been transmitted by the tag, one or more intended receivers must reliably detect and decode the transmission. As the intended receivers do not know a priori when the transmission begins, symbol detection must be performed asynchronously. An observation interval is defined as the length-$NM$ vector $\mathbf{y}(\ell) = [\, y(\ell) \quad y(\ell-1) \quad y(\ell-NM+1)\,]^{\mathrm{T}}$ obtained by the receiver A/D. The receiver searches for a communication symbol over an observation interval $\gg NM$ [9]. Due to the nature of the embedded symbol, the receiver must perform filtering to suppress the clutter and coherently integrate the energy of the symbol (if present). The receive-filter bank is composed of $K$ filters, denoted $\mathbf{w}_k$, corresponding to each possible symbol.

The receiver generates a set of outputs from the filter bank, defined as $z_{y,k}(\ell) = \mathbf{w}_k^{\mathrm{H}}\mathbf{y}(\ell)$ [9]. The output of each filter forms a set $\{\, z_{y,1}(\ell) \quad z_{y,2}(\ell) \quad \cdots \quad z_{y,K}(\ell)\,\}$, for a collection of time samples indexed by $\ell$. This set is sorted to determine the magnitude of the greatest response for each filter, with the collection of maximum magnitudes providing the location in the observation interval for which each symbol has the highest probability of being present. Subsequently, the maximum over this set of $K$ values, denoted $|z_{y,\max}^{(k)}|$, is the magnitude of the most likely symbol to be present over the observation interval [9].

Formally, the receive filtering may be formulated as a multiple-hypothesis test where the $K+1$ hypotheses are expressed as

$$\begin{aligned} \mathcal{H}_0 &: \mathbf{y} = \mathbf{S}\mathbf{x} + \mathbf{u} \\ \mathcal{H}_k &: \mathbf{y} = \mathbf{S}\mathbf{x} + \alpha\mathbf{c}_k + \mathbf{u} \end{aligned} \tag{20}$$

for $k = 1, 2, \ldots, K$. Hypothesis $\mathcal{H}_k$ corresponds to the $k$th symbol being received, $\alpha$ is an unknown complex scaling factor that subsumes the transmitted symbol power $\gamma$, and $\mathcal{H}_0$ is the null hypothesis (no symbol present). The maximum output from the $k$ filters is

$$\left|z_{y,\max}^{(k)}\right| = \max_{k,\ell} \left|z_{y,k}\,(\ell)\right|, \tag{21}$$

such that the most likely symbol to be present in the observation interval is

$$\hat{k} = \arg\max_{k,\ell} \left|z_{y,k}\,(\ell)\right|. \tag{22}$$

To account for the null hypothesis and control the probability of false alarm, the receiver may use the filter outputs of the $K-1$ rejected symbols ($k \neq \hat{k}$) to characterize the filtered clutter and noise [9]. This characterization is then used to form a threshold $\mathcal{T}$ based on an acceptable probability of false alarm. If $|z_{y,\max}^{(k)}| > \mathcal{T}$, then the receiver decides that the $\hat{k}$th symbol is present in the observation interval. Otherwise, the receiver decides that no communication symbol is present. This two-stage process uses an adaptive Neyman–Pearson approach [15].

While the clutter process $x(t)$ is not known, we can assume that it is zero mean. If this assumption is met, the central limit theorem causes the linear transformation of $\mathbf{S}\mathbf{x}$ from (1), followed by the filtering $\mathbf{w}_k^{\mathrm{H}}\mathbf{y}(\ell)$, to result in complex Gaussian-distributed samples. Therefore, the filter output $|z_{y,k}(\ell)|$ can be approximated as independent and identically distributed Rayleigh samples. If no symbol is present, the probability of false alarm is given by the probability that the maximum value of $(K-1)L$ Rayleigh random variables exceeds a threshold. Under the assumption that the $(K-1)L$ samples are independent and identically distributed, the probability of false alarm is found from the cumulative distribution function of the Rayleigh distribution as [15]

$$\begin{aligned} F_Z\,(z;\sigma) &= \left[1 - \exp\left\{-\frac{z^2}{2\sigma^2}\right\}\right]^{(K-1)L}\Bigg|_{z=\mathcal{T}} \\ &= 1 - P_{\mathrm{fa}}. \end{aligned} \tag{23}$$

Rearranging, the Neyman–Pearson threshold $\mathcal{T}$ for the detector becomes

$$\mathcal{T} = \sqrt{-2\sigma_z^2 \ln\left[1 - (1 - P_{\mathrm{fa}})^{\frac{1}{(K-1)L}}\right]}, \tag{24}$$

where $\sigma_z$ is the Rayleigh scale parameter. The maximum-likelihood estimator of $\sigma_z$ is given as [16]

$$\hat{\sigma} = \sqrt{\frac{1}{2\,(K-1)\,L} \sum_{j=1,\, j\neq\hat{k}}^{K} \sum_{\ell=1}^{L} \left|z_{y,j}\,(\ell)\right|^2}. \tag{25}$$

The maximum-likelihood estimator in (25) is biased, and the expected value can be expressed as [16]

$$E\,[\hat{\sigma}\,] \approx \sigma_z \left(1 - \frac{1}{8\,(K-1)\,L}\right). \tag{26}$$

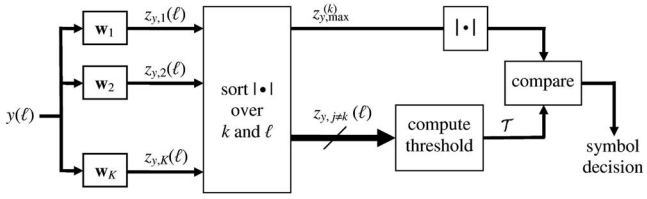


Fig. 6. Two-stage Neyman–Pearson detector [9].

However, (26) asymptotically approaches an unbiased estimate, and $(K-1)L$ can be assumed to be large.[1] The final detector output is

$$\text{symbol decision} = \begin{cases} k^{\text{th}}\,\text{symbol}, & \text{if } \left|z_{y,\max}^{(k)}\right| > \mathcal{T} \\ \text{no symbol}, & \text{otherwise} \end{cases} \tag{27}$$

and the overall two-stage detector is summarized in Fig. 6.

## IV. RECEIVE FILTERING

The approach to receive filtering in [7] drew inspiration from the rich spread-spectrum literature, as well as noting the special circumstances inherent to radar-embedded communications. Due to the high transmit power used by a typical radar system, the received clutter power is assumed to be large relative to the noise, so that the interference structure can be estimated. With this assumption in hand, [9] used a diagonally loaded decorrelating filter [17, 18] with the filter corresponding to the $k$th symbol given as

$$\mathbf{w}_k = \left(\mathbf{S}\mathbf{S}^{\mathrm{H}} + \lambda_{m+1}\mathbf{I}\right)^{-1}\mathbf{c}_k, \tag{28}$$

for $k = 1, 2, \ldots, K$, where the diagonal loading term $\lambda_{m+1}$ is the largest nondominant eigenvalue from (7). The diagonal loading was introduced for mathematical convenience in the analysis of the filter performance and to prevent noise enhancement effects.

To examine the performance of the decorrelating filter of (28), the analysis conducted in [9] derived the processing gain

$$\Delta = \frac{\text{SINR}_{\text{o}}}{\text{SINR}_{\text{i}}}, \tag{29}$$

where $\text{SINR}_{\text{i}}$ corresponds to the incident communication signal, clutter, and noise, and $\text{SINR}_{\text{o}}$ results from receive filtering. The processing gain for the DP symbol design in (9)—aside from the new scale factor $\beta$—combined with the decorrelating filter of (28) was derived in [9]. Here we examine the processing gain that results from using the DP (9), SDP (13), and SWF (18) symbol-design methods in conjunction with three prospective filtering schemes. Recall that for the extreme case of $m = 0$, the DP method provides the processing gain for the DSSS method. Similarly, for $m = NM$ the SWF design method has the same processing gain as the WF symbol design of (15). The filter structures examined here are the matched filter, the decorrelating filter, and a modification to the diagonally loaded decorrelating filter.

While each filter will be explored in conjunction with the symbol-design methods, the general definitions are given here. The familiar matched filter is defined as

$$\mathbf{w}_{\text{MF},k} = \mathbf{c}_k, \tag{30}$$

and the decorrelating-filter structure is

$$\begin{aligned} \mathbf{w}_{\text{DF},k} &= \left(\mathbf{S}\mathbf{S}^{\mathrm{H}}\right)^{-1}\mathbf{c}_k \\ &= \mathbf{V}\mathbf{\Lambda}^{-1}\mathbf{V}^{\mathrm{H}}\mathbf{c}_k. \end{aligned} \tag{31}$$

Assuming the receiver can determine the clutter and noise power, we also consider a different loaded decorrelating filter (LDF) useful for analysis purposes, which is defined as

$$\mathbf{w}_{\text{LDF},k} = \mathbf{V}\tilde{\mathbf{\Lambda}}^{-1}\mathbf{V}^{\mathrm{H}}\mathbf{c}_k, \tag{32}$$

where the modified eigenvalue matrix is

$$\tilde{\mathbf{\Lambda}} = \sigma_x^2\mathbf{\Lambda} + \sigma_u^2\mathbf{I}. \tag{33}$$

The incident SINR at the receiver can be found via examination of the squared magnitude $\|\mathbf{y}\|^2$ of the received signal, where the dependence on $\ell$ is excluded for brevity. The expectation of the squared magnitude of the received signal when a symbol is present is [9]

$$\begin{aligned} E\left[\|\mathbf{y}\|^2\right] &= E\left[(\mathbf{S}\mathbf{x} + \alpha\mathbf{c}_k + \mathbf{u})^{\mathrm{H}}(\mathbf{S}\mathbf{x} + \alpha\mathbf{c}_k + \mathbf{u})\right] \\ &= E\left[(\mathbf{S}\mathbf{x})^{\mathrm{H}}(\mathbf{S}\mathbf{x})\right] + E\left[(\alpha\mathbf{c}_k)^{\mathrm{H}}(\alpha\mathbf{c}_k)\right] + E\left[\mathbf{u}^{\mathrm{H}}\mathbf{u}\right] \\ &= R_{\text{i}} + S_{\text{i}} + N_{\text{i}}, \end{aligned} \tag{34}$$

assuming the noise and clutter process are zero mean and uncorrelated, and where $\alpha$ subsumes transmit gain and propagation path loss. The term $R_{\text{i}}$ represents the incident clutter power, $S_{\text{i}}$ is the incident signal power, and $N_{\text{i}}$ is the incident noise power. All symbol-design methods included a scaling term, resulting in

$$S_{\text{i}} = |\alpha|^2, \tag{35}$$

while the interference power and noise power are given, respectively, as

$$\begin{aligned} R_{\text{i}} &= \sigma_x^2 \text{tr}\{\mathbf{\Lambda}\} \\ &= \sigma_x^2 NM \end{aligned} \tag{36}$$

and

$$N_{\text{i}} = \sigma_u^2 NM. \tag{37}$$

Thus in general the incident (input) SINR is

$$\text{SINR}_{\text{i}} = \frac{|\alpha|^2}{NM\left(\sigma_x^2 + \sigma_u^2\right)}. \tag{38}$$

For an arbitrary filter $\mathbf{w}_k$, the output SINR is found from the expression

$$\begin{aligned} &E\left[\left|\mathbf{w}_k^{\mathrm{H}}\mathbf{y}\right|^2\right] \\ &\quad = E\left[(\mathbf{S}\mathbf{x} + \alpha\mathbf{c}_k + \mathbf{u})^{\mathrm{H}}\mathbf{w}_k\mathbf{w}_k^{\mathrm{H}}(\mathbf{S}\mathbf{x} + \alpha\mathbf{c}_k + \mathbf{u})\right] \end{aligned}$$

[1] Note that in [9], the threshold dependence is erroneously given as the maximum of a single Rayleigh random variable rather than $(K-1)L$ samples. However, the Rayleigh distribution possesses a light tail. For the examples in [9], the threshold should be only ~1.2 dB higher to meet the desired $P_{\text{fa}}$ of $10^{-5}$.

$$= E\left[(\mathbf{Sx})^{\mathrm{H}}\mathbf{w}_k\mathbf{w}_k^{\mathrm{H}}(\mathbf{Sx})\right] + E\left[(\alpha\mathbf{c}_k)^{\mathrm{H}}\mathbf{w}_k\mathbf{w}_k^{\mathrm{H}}(\alpha\mathbf{c}_k)\right] + E\left[\mathbf{u}^{\mathrm{H}}\mathbf{w}_k\mathbf{w}_k^{\mathrm{H}}\mathbf{u}\right]$$
$$= R_{\mathrm{o}} + S_{\mathrm{o}} + N_{\mathrm{o}}. \tag{39}$$

The combination of symbol structure and receive filter determines the processing gain of the receiver. The output SINR is defined as

$$\mathrm{SINR}_{\mathrm{o}} = \frac{S_{\mathrm{o}}}{R_{\mathrm{o}} + N_{\mathrm{o}}}, \tag{40}$$

where the clutter power after filtering is, from (39),

$$\begin{aligned} R_{\mathrm{o}} &= E\left[(\mathbf{Sx})^{\mathrm{H}}\mathbf{w}_k\mathbf{w}_k^{\mathrm{H}}(\mathbf{Sx})\right] \\ &= E\left[\mathbf{w}_k^{\mathrm{H}}\mathbf{S}\mathbf{x}\mathbf{x}^{\mathrm{H}}\mathbf{S}^{\mathrm{H}}\mathbf{w}_k\right] \\ &= \mathbf{w}_k^{\mathrm{H}}\mathbf{S}E\left[\mathbf{x}\mathbf{x}^{\mathrm{H}}\right]\mathbf{S}^{\mathrm{H}}\mathbf{w}_k \\ &= \sigma_x^2\mathbf{w}_k^{\mathrm{H}}\mathbf{S}\mathbf{S}^{\mathrm{H}}\mathbf{w}_k \\ &= \sigma_x^2\mathbf{w}_k^{\mathrm{H}}\mathbf{V}\mathbf{\Lambda}\mathbf{V}^{H}\mathbf{w}_k \end{aligned} \tag{41}$$

and the noise power after filtering is similarly

$$\begin{aligned} N_{\mathrm{o}} &= E\left[\mathbf{u}^{\mathrm{H}}\mathbf{w}_k\mathbf{w}_k^{\mathrm{H}}\mathbf{u}\right] \\ &= E\left[\mathrm{tr}\left\{\mathbf{w}_k^{\mathrm{H}}\mathbf{u}\mathbf{u}^{\mathrm{H}}\mathbf{w}_k\right\}\right] \\ &= \mathrm{tr}\left\{\mathbf{w}_k^{\mathrm{H}}E\left[\mathbf{u}\mathbf{u}^{\mathrm{H}}\right]\mathbf{w}_k\right\} \\ &= \sigma_u^2\mathbf{w}_k^{\mathrm{H}}\mathbf{w}_k. \end{aligned} \tag{42}$$

The signal power must be determined separately for each symbol type. The processing gain for each symbol design and filter structure is derived in Appendix A.

Let us now examine the processing gains afforded by the various combinations of symbol design and filter structure. As was the case in Section II-E, the radar waveform is a linearly frequency-modulated chirp with time-bandwidth product $N = 64$ and an oversampling factor (relative to the 3 dB bandwidth) of $M = 2$. We consider two scenarios. First is the typical case of high CNR, here set to 30 dB. Second, we consider the case of CNR = 0 dB, where the clutter power is equal to the noise power. As the symbol designs and filters are constructed to take advantage of the masking interference provided by the radar clutter, a CNR of 0 dB provides a worst-case scenario of the processing gain for each combination of symbol and filter.

For the baseline case of DSSS symbol generation, the MF produces a gain equal to the time-bandwidth product of the symbol (which is $2 \times 64 = 128$, or 21.1 dB). For a CNR of 30 dB, LDF and DF filtering of the DSSS symbol both produce a processing gain of 35.74 dB by virtue of clutter cancellation. Alternatively, for a CNR of 0 dB, the LDF provides a processing gain of 22.2 dB and the DF provides a processing gain of 19.4 dB. Therefore, for both high and low CNRs, the LDF provides an advantage over the MF and DF if the clutter and noise powers are accurately estimated.

Figs. 7–9 show the processing gains for the DP, SDP, and SWF symbol designs for each of the three filter structures. The high-CNR (30 dB) case is denoted by solid lines, while the low-CNR (0 dB) case is shown with dotted lines. For the high-CNR case, the clutter degrades MF performance. However, at low CNR the MF is comparable

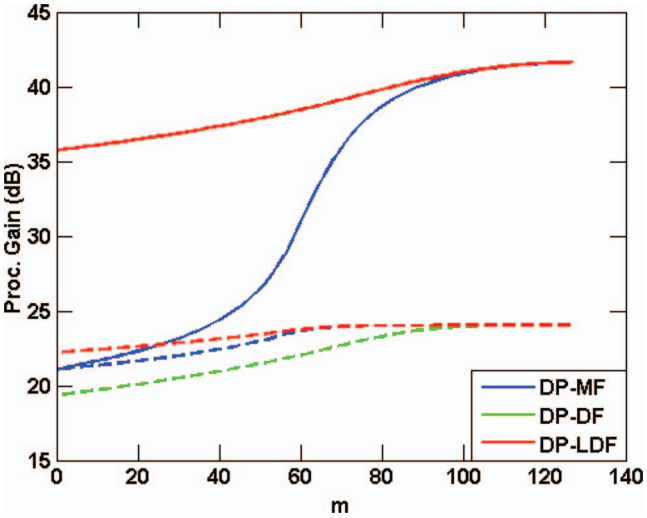


Fig. 7. Analytical processing gain for DP symbol for different receive filters, with high (solid) and low (dashed) CNR.

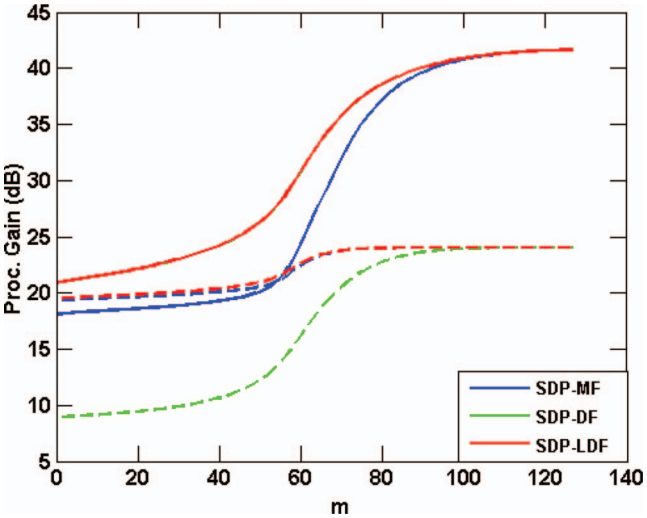


Fig. 8. Analytical processing gain for SDP symbol for different receive filters, with high (solid) and low (dashed) CNR.

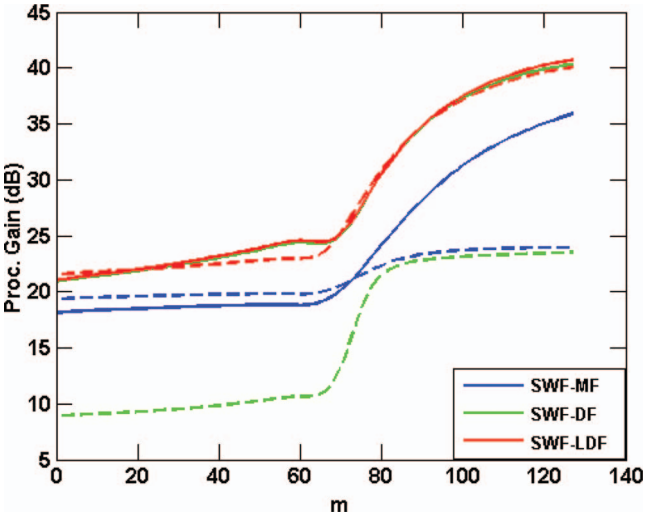


Fig. 9. Analytical processing gain for SWF symbol for different receive filters, with high (solid) and low (dashed) CNR.

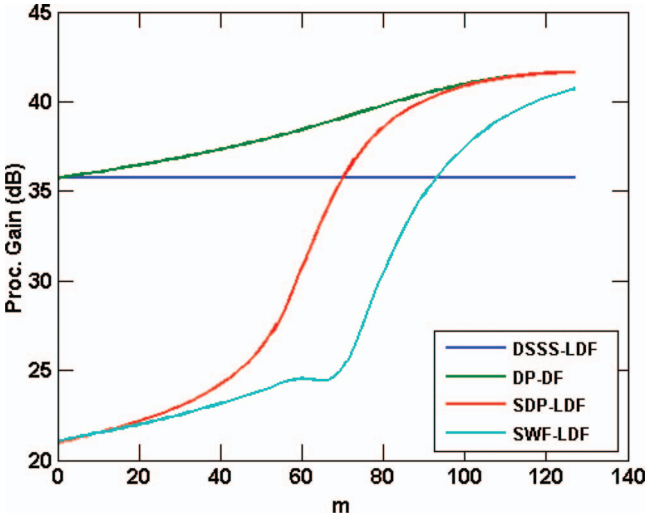


Fig. 10. Comparison of processing gains for high-CNR condition.

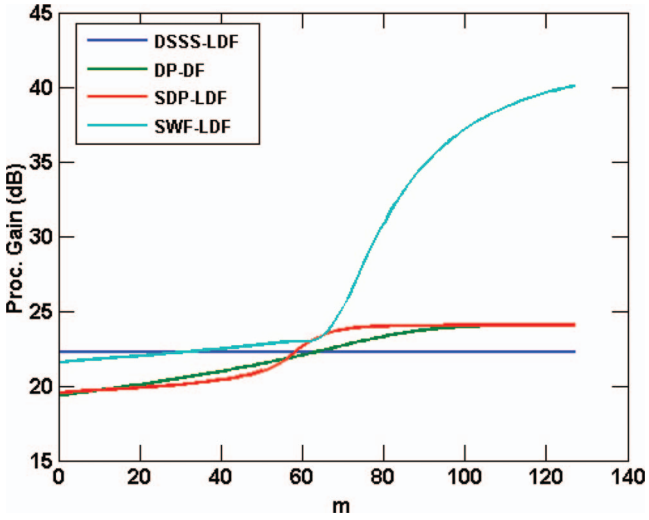


Fig. 11. Comparison of processing gains for low-CNR condition.

to the DF and LDF filter structures. Comparing Figs. 7 and 8, when DP symbols are used in conjunction with the DF or LDF, the processing gain is less sensitive to the size of the dominant subspace than when the SDP symbols are used.

Fig. 9 gives the processing gains for the SWF symbols when MF, DF, and LDF are used. For the high-CNR case, the DF and LDF are comparable and provide superior gain when compared to the MF. However, for the low-CNR case, filtering with the MF and DF yields processing-gain values that approach the coherent processing gain. However, the LDF is largely unaffected, regardless of whether the CNR is high or low. Therefore, the LDF is the best filter design to use in conjunction with the SWF symbol.

Fig. 10 compares the processing gain of the three proposed symbol-design methods at a CNR of 30 dB. The SDP and SWF symbols are filtered with the LDF, while due to the behavior at high values of $m$ we filter the DP symbol with the DF. Note that the DP symbol offers a higher processing gain than the DSSS symbol at all values of $m$, while the SDP and SWF symbols enjoy a higher processing gain only for large values of $m$.

Fig. 11 compares the processing gain for a CNR of 0 dB. In this case the DP and SDP methods enjoy $\approx$3 dB gain advantage over the traditional DSSS method. However, as was shown in Fig. 9, the processing gain is largely unaffected by the clutter power when the SWF symbol is used in conjunction with the LDF.

## V. INTERCEPT AND DETECTION EVALUATION

Section IV-A compared the processing gain afforded by the various combinations of symbol designs and filter structures. Here, Monte Carlo simulations are used to examine the probabilities of detection and intercept. In particular, we establish the ability of the two-stage NP receiver of Fig. 6 to asynchronously detect the correct transmitted symbol and compare it to the capability of an intercept receiver to detect whether a symbol is present.

### A. Intercept Receiver

Where Fig. 10 shows the high processing gain of the SDP and DP symbols when the size of the nondominant subspace is small ($m$ is large), Fig. 4 shows that the resulting spectral response of such symbols is high where the masking clutter is low. Thus the possible processing-gain enhancement for a particular symbol design must be tempered by the associated LPI nature that it represents. To examine the LPI property we use the intercept metric proposed in [9], defined as

$$\epsilon(\tilde{m}) = \mathbf{y}^{\mathrm{H}}\mathbf{P}_{\tilde{m}}\mathbf{y}, \tag{43}$$

where the projection matrix $\mathbf{P}_{\tilde{m}}$ is

$$\mathbf{P}_{\tilde{m}} = \mathbf{V}_{\mathrm{ND},\tilde{m}}\mathbf{V}_{\mathrm{ND},\tilde{m}}^{\mathrm{H}} \tag{44}$$

for $\tilde{m} \in [0, NM]$.

In other words, the intercept receiver progressively projects out the dominant subspace and then performs energy detection. The full-space (i.e., $\tilde{m} = 0$) response of (43) coincides with the classic total-power radiometer [11]. When the intercept receiver projects out the 3 dB bandwidth of the radar waveform (i.e., $\tilde{m} = N$), (43) is a subspace implementation of the interference-nulling detector of [11].

To provide a worst-case assessment from a covert communication-system perspective, we assume that the intercept receiver possesses knowledge of several transmission parameters that would not necessarily be available to it in practice. Namely, the intercept receiver knows the oversampling factor $M$ and the time-bandwidth product $N$. In addition, we assume that the intercept receiver knows the size of the dominant subspace (i.e., $\tilde{m} = m$) and has clairvoyant knowledge of the proper detection threshold to maintain the desired false-alarm rate.

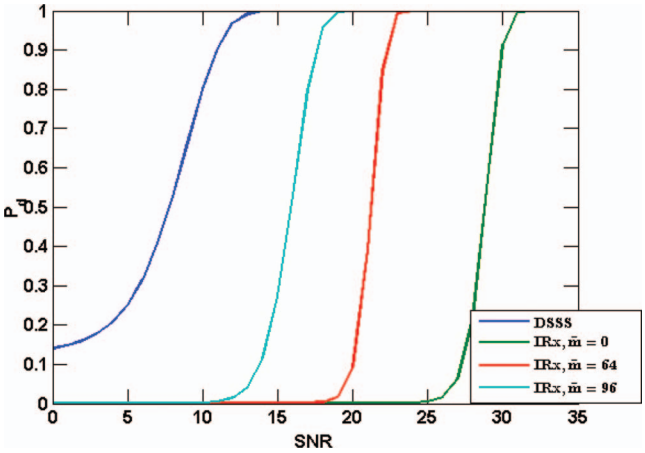


Fig. 12. Probability of detection and intercept for DSSS symbol (not using masking radar clutter).

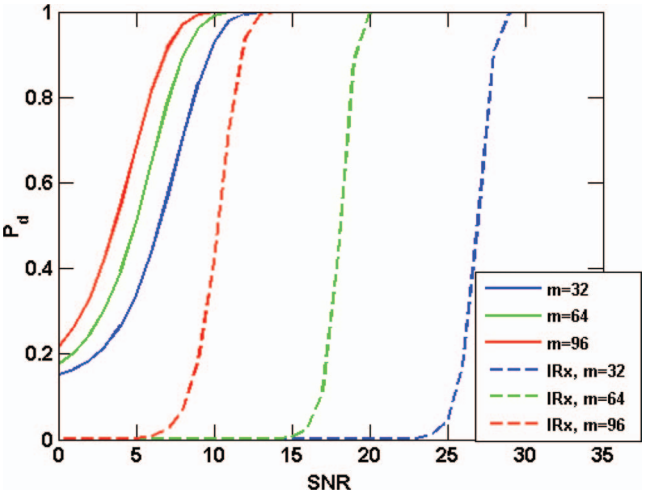


Fig. 13. Probability of detection and intercept for DP symbol.

## B. Probability of Detection Analysis

We again consider a linearly frequency-modulated radar waveform with a time-bandwidth product of $N = 64$ that is oversampled by a factor of $M = 2$. A symbol alphabet size of $K = 8$ was chosen, yielding $\log_2(K) = 3$ bits/symbol. To provide a high-fidelity estimate, the communication symbols are up-sampled by a factor of 4 to simulate the continuous transmission of a communication waveform. All clutter and noise is added at this "continuous" stage and the SNR and CNR are set in the continuous domain. The CNR is 30 dB for all cases. The resultant symbols are decimated by 4 to provide a sampled discrete input to the two-stage NP receiver and intercept receiver. In all cases, the NP receiver and intercept receiver maintain $P_{\text{fa}} = 10^{-5}$. Both the desired and intercept receivers scan over an observation interval of $L = 3NM$ samples to determine if a symbol is present. To provide a metric of LPI performance, we consider the difference in SNR required for successful detection of a symbol by the NP receiver compared to the partially clairvoyant intercept receiver. This difference in SNR required for successful detection is the gain advantage of the desired receiver.

Fig. 12 illustrates the probability of detection for a DSSS symbol. The desired receiver uses an LDF. We compare three different intercept-receiver parameterizations: $\tilde{m} = 0$, 64, and 96. The cases of $\tilde{m} = 0$ and $\tilde{m} = N = 64$ correspond to the total-power radiometer and interference-canceling receivers of [11], respectively. However, in [11] the interference source occupies a relatively narrow bandwidth with respect to the transmitted symbol. As was shown in Figs. 2 –4, the clutter response possesses a large spectral roll-off, which helps to mask the communication symbol when $\tilde{m} = N$. Therefore, the $\tilde{m} = 96$ case is included, which eliminates most of the clutter response while still leaving a significant portion ($\approx$25%) of the symbol power. Fig. 12 illustrates the decrease in LPI performance when the intercept receiver eliminates increasing amounts of the clutter. However, the desired receiver still maintains a gain advantage of $\approx$6 dB over the intercept receiver, even when the majority of the clutter is canceled.

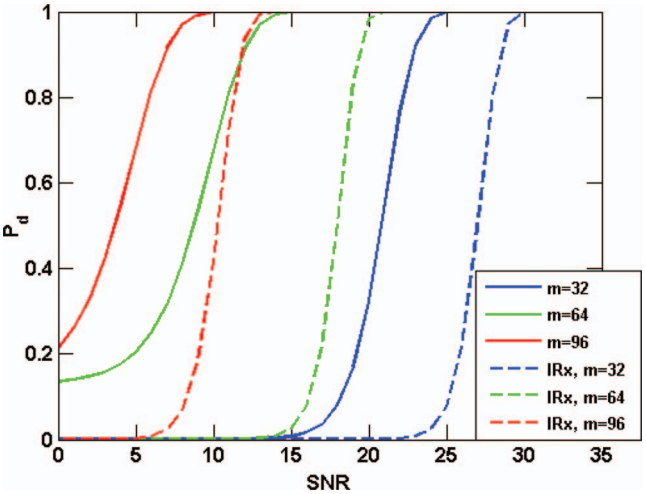


Fig. 14. Probability of detection and intercept for SDP symbol.

Fig. 13 verifies the relatively low amount of processing-gain variance (as a function of $m$) for the DP/DF combination that was observed in Fig. 7. However, note that while transmitting in a portion of the clutter subspace degrades detection performance, it greatly affects intercept performance. The desired receiver enjoys an $\approx$4 dB advantage over the intercept receiver when $m = 96$ versus an $\approx$17 dB advantage when $m = 32$.

The heavy dependence of processing gain on $m$ for the SDP symbol is shown in Fig. 14, where the desired receiver uses an LDF. For the SDP symbol design, the choice of $m = 64$ yields the largest gain advantage for the desired receiver. The spectral shaping of the SDP symbol at $m = 64$ (as was illustrated in Fig. 3) only reduces intercept performance by $\approx$1 dB in relation to the DP symbol. Further, the lower processing gain at the same value of $m$ reduces the detection probability at the desired

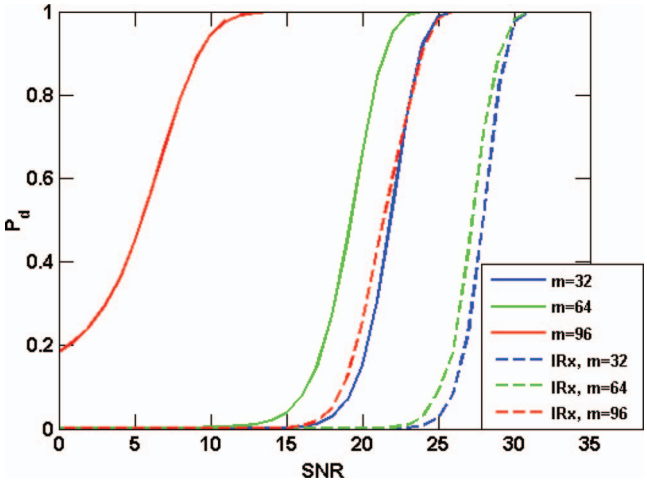


Fig. 15. Probability of detection and intercept for SWF symbol.

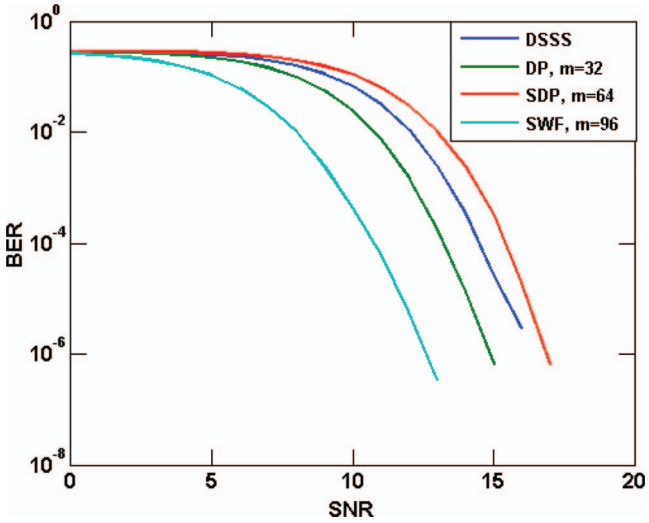


Fig. 16. BER comparison for notable symbol/filter combinations.

receiver. Therefore, the increased processing gain afforded by the DP symbol design outweighs the smaller LPI advantage of the SDP symbol design, meaning that spectral shaping alone does not appear to be beneficial.

Fig. 15 illustrates the detection characteristics of the SWF symbol design when the desired receiver uses the LDF. The similarities between the SDP and SWF symbols at $m = 32$ and 64 (as shown in Figs. 2 and 3) carry through to the probability-of-detection analysis in Figs. 14 and 15. However, when $m = 96$ the SWF symbol deviates significantly from the DP and SDP symbols. Recall from Fig. 4 that the SWF symbol at $m = 96$ allocates reduced power in the clutter subspace (relative to the DSSS symbol) but does not null the clutter subspace like the DP and SDP symbols. The majority of the transmit-power allocation occurs in the roll-off region, and significantly less ($\approx -10$ dB with respect to the DSSS symbol, $\approx -16$ dB with respect to the DP/SDP symbols) transmit power is allocated at the outer edges of the noise subspace. This behavior allows for $\approx$14 dB of gain advantage for the desired receiver, while maintaining the large amount of processing gain shown in Fig. 9. As such, one can infer that a judicious spectral distribution of symbol power is one that properly balances between interference avoidance to maximize probability of detection (such as WF provides) and maintenance of interference similarity for low probability of intercept.

Finally, in Fig. 16 we examine the bit error rates (BER) for the best-performing combinations of symbol design and filter (with respect to the gain advantage). When the DP symbol is transmitted, the desired receiver uses the DF, while the LDF is used when the DSSS, SDP, or SWF symbol is transmitted. In particular, note that the SWF symbol design provides $\approx$2–3 dB of gain over the DP method for a similar BER. Both the SWF and DP symbol designs provide substantial LPI improvements over the DSSS method of symbol design, as well as requiring less power to achieve the same BER.

## VI. CONCLUSION

Several subspace-based symbol-design strategies have been presented and examined for LPI communication in the presence of high-power radar emissions. Such subspace strategies are inherently insensitive to timing differences and multipath. Here the previous subspace symbol-design methodology was extended to include spectral information in two separate ways: via spectral shaping according to the radar-induced clutter response and using the well-known principle of water filling. The purpose of considering these new symbol structures is to ascertain beneficial symbol attributes that may balance between good communication performance and low intercept probability within a litany of practical constraints.

Using multiple receive-filtering structures, each of the proposed symbol designs was analytically evaluated in terms of processing gain relative to the masking radar interference. Further, based on the use of a presumed worst-case partially clairvoyant intercept receiver, the gain advantage of each symbol design was evaluated. This analysis shows that a hybrid combination of water filling and spectral shaping (according to the roll-off region) provides a good compromise between interference avoidance and maintenance of interference similarity that should inform the subsequent design of robust optimal symbols.

## APPENDIX A. PROCESSING-GAIN DERIVATIONS

The processing gain for the three symbol-design methods is derived here for each of the filter structures under consideration.

### A. Processing Gain of DP Symbols

When the DP symbol design of (9) is used in conjunction with an MF, the output symbol power is found

from (11) and (39) as

$$S_{\mathrm{o,DP-MF}} = |\alpha|^2 \left|\mathbf{w}^{\mathrm{H}}_{\mathrm{DP-MF},k}\mathbf{c}_{\mathrm{DP},k}\right|^2 = |\alpha|^2 \left|\mathbf{c}^{\mathrm{H}}_{\mathrm{DP},k}\mathbf{c}_{\mathrm{DP},k}\right|^2 = |\alpha|^2, \tag{45}$$

and the filtered interference and noise powers are found from (9), (10), (41), and (42) to be

$$\begin{aligned} R_{\mathrm{o,DP-MF}} &= \sigma_x^2 \mathbf{w}^{\mathrm{H}}_{\mathrm{DP-MF},k}\mathbf{V}\boldsymbol{\Lambda}\mathbf{V}^{\mathrm{H}}\mathbf{w}_{\mathrm{DP-MF},k} \\ &= \sigma_x^2 \beta_{\mathrm{DP},m}\mathbf{q}^{\mathrm{H}}_{\mathrm{ND},k}\mathbf{V}^{\mathrm{H}}_{\mathrm{ND},m}\mathbf{V}\boldsymbol{\Lambda}\mathbf{V}^{\mathrm{H}}\mathbf{V}_{\mathrm{ND},m}\mathbf{q}_{\mathrm{ND},k} \\ &\approx \sigma_x^2 \frac{\mathrm{tr}\left\{\boldsymbol{\Lambda}_{\mathrm{ND},m}\right\}}{NM-m} \end{aligned} \tag{46}$$

and

$$\begin{aligned} N_{\mathrm{o,DP-MF}} &= \sigma_u^2 \mathbf{w}^{\mathrm{H}}_{\mathrm{DP-MF},k}\mathbf{w}_{\mathrm{DP-MF},k} \\ &= \sigma_u^2 \beta_{\mathrm{DP},m}\mathbf{q}^{\mathrm{H}}_{\mathrm{ND},k}\mathbf{V}^{\mathrm{H}}_{\mathrm{ND},m}\mathbf{V}_{\mathrm{ND},m}\mathbf{q}_{\mathrm{ND},k} \\ &\approx \sigma_u^2, \end{aligned} \tag{47}$$

respectively. Substituting (45)–(47) into (40), the output SINR when a DP symbol is filtered through a matched filter is

$$\mathrm{SINR}_{\mathrm{o,DP-MF}}(m) = \frac{|\alpha|^2}{\sigma_x^2 \frac{\mathrm{tr}\{\boldsymbol{\Lambda}_{\mathrm{ND},m}\}}{NM-m} + \sigma_u^2}. \tag{48}$$

Therefore, from (38) and (48), the processing gain afforded by using MF with DP symbols is

$$\Delta_{\mathrm{DP-MF}}(m) = \frac{NM\left(\sigma_x^2+\sigma_u^2\right)}{\sigma_x^2 \frac{\mathrm{tr}\{\boldsymbol{\Lambda}_{\mathrm{ND},m}\}}{NM-m} + \sigma_u^2}. \tag{49}$$

Substituting (9) into (31), the DF for a DP symbol takes the form

$$\begin{aligned} \mathbf{w}_{\mathrm{DP-DF},k} &= \mathbf{V}\boldsymbol{\Lambda}^{-1}\mathbf{V}^{\mathrm{H}}\left(\beta^{1/2}_{\mathrm{DP},m}\mathbf{V}_{\mathrm{ND},m}\mathbf{q}_{\mathrm{ND},k}\right) \\ &= \beta^{1/2}_{\mathrm{DP},m}\mathbf{V}\begin{bmatrix}\mathbf{0}_{m\times(NM-m)} \\ \boldsymbol{\Lambda}^{-1}_{\mathrm{ND}}\end{bmatrix}\mathbf{q}_{\mathrm{ND},k}. \end{aligned} \tag{50}$$

The signal power after processing a DP symbol with the filter of (50) is found from (9) and (12) to be

$$\begin{aligned} &S_{\mathrm{o,DP-DF}} \\ &= |\alpha|^2 \left|\mathbf{w}^{\mathrm{H}}_{\mathrm{DP-DF},k}\mathbf{c}_{\mathrm{DP},k}\right|^2 \\ &= |\alpha|^2 \left|\beta_{\mathrm{DP},m}\mathbf{q}^{\mathrm{H}}_{\mathrm{ND},k}\left[\mathbf{0}_{(NM-m)\times m}\,\middle|\,\boldsymbol{\Lambda}^{-1}_{\mathrm{ND}}\right]\mathbf{V}^{\mathrm{H}}\mathbf{V}_{\mathrm{ND},m}\mathbf{q}_{\mathrm{ND},k}\right|^2 \\ &\approx \frac{|\alpha|^2\beta^2_{\mathrm{DP},m}}{(NM)^2}\left(\mathrm{tr}\left\{\boldsymbol{\Lambda}^{-1}_{\mathrm{ND},m}\right\}\right)^2 \\ &= \frac{|\alpha|^2\left(\mathrm{tr}\left\{\boldsymbol{\Lambda}^{-1}_{\mathrm{ND},m}\right\}\right)^2}{(NM-m)^2}. \end{aligned} \tag{51}$$

Using (10), (12), and (41), the interference power after filtering with the DF of (50) is

$$\begin{aligned} R_{\mathrm{o,DP-DF}} &= \sigma_x^2 \mathbf{w}^{\mathrm{H}}_{\mathrm{DP-DF},k}\mathbf{V}\boldsymbol{\Lambda}\mathbf{V}^{\mathrm{H}}\mathbf{w}_{\mathrm{DP-DF},k} \\ &= \sigma_x^2 \beta_{\mathrm{DP},m}\mathbf{q}^{\mathrm{H}}_{\mathrm{ND},k}\left[\mathbf{0}\,\middle|\,\boldsymbol{\Lambda}^{-1}_{\mathrm{ND}}\right]\boldsymbol{\Lambda}\begin{bmatrix}\mathbf{0} \\ \boldsymbol{\Lambda}^{-1}_{\mathrm{ND}}\end{bmatrix}\mathbf{q}_{\mathrm{ND},k} \\ &\approx \sigma_x^2 \frac{\mathrm{tr}\left\{\boldsymbol{\Lambda}^{-1}_{\mathrm{ND},m}\right\}}{NM-m}; \end{aligned} \tag{52}$$

and using (10), (12), and (42), the noise power is

$$\begin{aligned} N_{\mathrm{o,DP-DF}} &= \sigma_u^2 \mathbf{w}^{\mathrm{H}}_{\mathrm{DP-DF},k}\mathbf{w}_{\mathrm{DP-DF},k} \\ &= \sigma_u^2 \beta_{\mathrm{DP},m}\mathbf{q}^{\mathrm{H}}_{\mathrm{ND},k}\left[\mathbf{0}\,\middle|\,\boldsymbol{\Lambda}^{-1}_{\mathrm{ND}}\right]\mathbf{V}^{\mathrm{H}}\mathbf{V}\begin{bmatrix}\mathbf{0} \\ \boldsymbol{\Lambda}^{-1}_{\mathrm{ND}}\end{bmatrix}\mathbf{q}_{\mathrm{ND},k} \\ &\approx \sigma_u^2 \frac{\mathrm{tr}\left\{\boldsymbol{\Lambda}^{-2}_{\mathrm{ND},m}\right\}}{NM-m}. \end{aligned} \tag{53}$$

Combining the results of (51)–(53) yields the output SINR

$$\mathrm{SINR}_{\mathrm{o,DP-DF}}(m) = \frac{|\alpha|^2\left(\mathrm{tr}\left\{\boldsymbol{\Lambda}^{-1}_{\mathrm{ND},m}\right\}\right)^2}{(NM-m)\left(\sigma_x^2\mathrm{tr}\left\{\boldsymbol{\Lambda}^{-1}_{\mathrm{ND},m}\right\}+\sigma_u^2\mathrm{tr}\left\{\boldsymbol{\Lambda}^{-2}_{\mathrm{ND},m}\right\}\right)}. \tag{54}$$

Relative to (38), the processing gain of the DF/DP combination is then

$$\Delta_{\mathrm{DP-DF}}(m) = \frac{NM\left(\sigma_x^2+\sigma_u^2\right)\left(\mathrm{tr}\left\{\boldsymbol{\Lambda}^{-1}_{\mathrm{ND},m}\right\}\right)^2}{(NM-m)\left(\sigma_x^2\mathrm{tr}\left\{\boldsymbol{\Lambda}^{-1}_{\mathrm{ND},m}\right\}+\sigma_u^2\mathrm{tr}\left\{\boldsymbol{\Lambda}^{-2}_{\mathrm{ND},m}\right\}\right)}. \tag{55}$$

The third filter structure we consider for the DP symbols is the LDF of (32). For a DP symbol, (32) becomes

$$\begin{aligned} \mathbf{w}_{\mathrm{DP-LDF},k} &= \mathbf{V}\tilde{\boldsymbol{\Lambda}}^{-1}\mathbf{V}^{\mathrm{H}}\left(\beta^{1/2}_{\mathrm{DP},m}\mathbf{V}_{\mathrm{ND},m}\mathbf{q}_{\mathrm{ND},k}\right) \\ &= \beta^{1/2}_{\mathrm{DP},m}\mathbf{V}\begin{bmatrix}\mathbf{0} \\ \tilde{\boldsymbol{\Lambda}}^{-1}_{\mathrm{ND}}\end{bmatrix}\mathbf{q}_{\mathrm{ND},k}. \end{aligned} \tag{56}$$

Following similar derivations as in (51)–(53), it can be shown that a DP symbol filtered through the LDF of (56) has an expected SINR of

$$\mathrm{SINR}_{\mathrm{o,DP-LDF}}(m) = \frac{|\alpha|^2\left(\mathrm{tr}\left\{\tilde{\boldsymbol{\Lambda}}^{-1}_{\mathrm{ND},m}\right\}\right)^2}{(NM-m)\left(\sigma_x^2\mathrm{tr}\left\{\tilde{\boldsymbol{\Lambda}}^{-2}_{\mathrm{ND},m}\boldsymbol{\Lambda}_{\mathrm{ND},m}\right\}+\sigma_u^2\mathrm{tr}\left\{\tilde{\boldsymbol{\Lambda}}^{-2}_{\mathrm{ND},m}\right\}\right)}. \tag{57}$$

The processing gain of the LDF is then

$$\Delta_{\mathrm{DP-LDF}}(m) = \frac{NM\left(\sigma_x^2+\sigma_u^2\right)\left(\mathrm{tr}\left\{\tilde{\boldsymbol{\Lambda}}^{-1}_{\mathrm{ND},m}\right\}\right)^2}{(NM-m)\left(\sigma_x^2\mathrm{tr}\left\{\tilde{\boldsymbol{\Lambda}}^{-2}_{\mathrm{ND},m}\boldsymbol{\Lambda}_{\mathrm{ND},m}\right\}+\sigma_u^2\mathrm{tr}\left\{\tilde{\boldsymbol{\Lambda}}^{-2}_{\mathrm{ND},m}\right\}\right)}. \tag{58}$$

### B. Processing Gain of SWF Symbols

The second symbol-design method under examination is the SWF method. As in (45), the scaling factor $\beta_{\mathrm{SWF}}$ causes the output power of an MF processing the SWF symbol of (18) to be the squared magnitude of the complex gain coefficient:

$$S_{\mathrm{o,SWF-MF}} = |\alpha|^2\left|\mathbf{w}^{\mathrm{H}}_{\mathrm{SWF-MF},k}\mathbf{c}_{\mathrm{SWF},k}\right|^2 = |\alpha|^2. \tag{59}$$

The interference and noise powers after MF with (18) are found from (41) and (42) to be, respectively,

$$\begin{aligned} R_{\text{o,SWF-MF}} &= \sigma_x^2 \mathbf{w}_{\text{SWF-MF},k}^{\text{H}} \mathbf{V}\boldsymbol{\Lambda}\mathbf{V}^{\text{H}} \mathbf{w}_{\text{SWF-MF},k} \\ &= \sigma_x^2 \beta_{\text{SWF},m} \mathbf{q}_k^{\text{H}} \boldsymbol{\Lambda}_{\text{P},m}^{1/2} \mathbf{V}^{\text{H}} \mathbf{V}\boldsymbol{\Lambda}\mathbf{V}^{\text{H}} \mathbf{V} \boldsymbol{\Lambda}_{\text{P},m}^{1/2} \mathbf{q}_k \\ &\approx \sigma_x^2 \frac{\text{tr}\left\{\boldsymbol{\Lambda}_{\text{P},m}\boldsymbol{\Lambda}\right\}}{\text{tr}\left\{\boldsymbol{\Lambda}_{\text{P},m}\right\}} \\ &= \sigma_x^2 \frac{m + \text{tr}\left\{\boldsymbol{\Lambda}_{\text{ND},m}^2\right\}}{\text{tr}\left\{\boldsymbol{\Lambda}_{\text{P},m}\right\}} \end{aligned} \tag{60}$$

and

$$N_{\text{o,SWF-M}F} = \sigma_u^2 \mathbf{w}_{\text{SWF-MF},k}^{\text{H}} \mathbf{w}_{\text{SWF-MF},k} = \sigma_u^2. \tag{61}$$

Combining (59)–(61), the SINR after processing an SWF symbol with an MF is

$$\text{SINR}_{\text{o,SWF-MF}}(m) = \frac{|\alpha|^2}{\sigma_x^2 \frac{m + \text{tr}\left\{\boldsymbol{\Lambda}_{\text{ND},m}^2\right\}}{\text{tr}\left\{\boldsymbol{\Lambda}_{\text{P},m}\right\}} + \sigma_u^2}, \tag{62}$$

so the resultant processing gain is

$$\Delta_{\text{SWF-MF}}(m) = \frac{NM\left(\sigma_x^2 + \sigma_u^2\right)}{\sigma_x^2 \frac{m + \text{tr}\left\{\boldsymbol{\Lambda}_{\text{ND},m}^2\right\}}{\text{tr}\left\{\boldsymbol{\Lambda}_{\text{P},m}\right\}} + \sigma_u^2}. \tag{63}$$

The DF corresponding to the SWF symbol is found by applying (18) to (31), giving

$$\begin{aligned} \mathbf{w}_{\text{SWF-DF},k} &= \mathbf{V}\boldsymbol{\Lambda}^{-1}\mathbf{V}^{\text{H}} \left(\beta_{\text{SWF},m}^{1/2} \mathbf{V}\boldsymbol{\Lambda}_{\text{P},m}^{1/2} \mathbf{q}_k\right) \\ &= \beta_{SWF,m}^{1/2} \mathbf{V}\boldsymbol{\Lambda}^{-1}\boldsymbol{\Lambda}_{\text{P},m}^{1/2} \mathbf{q}_k. \end{aligned} \tag{64}$$

From (18), filtering an SWF symbol with (64) yields an expected signal power of

$$\begin{aligned} S_{\text{o,SWF-DF}} &= |\alpha|^2 \left|\mathbf{w}_{\text{SWF-DF},k}^{\text{H}} \mathbf{c}_{\text{SWF},k}\right|^2 \\ &= |\alpha|^2 \left|\beta_{\text{SWF},m} \mathbf{q}_k^{\text{H}} \boldsymbol{\Lambda}_{\text{P},m}^{1/2} \boldsymbol{\Lambda}^{-1} \mathbf{V}^{\text{H}} \mathbf{V} \boldsymbol{\Lambda}_{\text{P},m}^{1/2} \mathbf{q}_k\right|^2 \\ &\approx \frac{|\alpha|^2 \beta_{\text{SWF},m}^2}{(NM)^2} \left(\text{tr}\left\{\boldsymbol{\Lambda}_{\text{P},m}\boldsymbol{\Lambda}^{-1}\right\}\right)^2 \\ &= \frac{|\alpha|^2 \left(\text{tr}\left\{\boldsymbol{\Lambda}_{\text{D}}^{-2}\right\} + NM - m\right)^2}{\left(\text{tr}\left\{\boldsymbol{\Lambda}_{\text{P},m}\right\}\right)^2}. \end{aligned} \tag{65}$$

From (41), the interference power after processing with the DF of (64) is

$$\begin{aligned} R_{\text{o,SWF-DF}} &= \sigma_x^2 \mathbf{w}_{\text{SWF-DF},k}^{\text{H}} \mathbf{V}\boldsymbol{\Lambda}\mathbf{V}^{\text{H}} \mathbf{w}_{\text{SWF-DF},k} \\ &= \sigma_x^2 \beta_{\text{SWF},m} \mathbf{q}_k^{\text{H}} \boldsymbol{\Lambda}_{\text{P},m}^{1/2} \boldsymbol{\Lambda}^{-1} \mathbf{V}^{\text{H}} \mathbf{V}\boldsymbol{\Lambda}\mathbf{V}^{\text{H}} \mathbf{V} \boldsymbol{\Lambda}^{-1} \boldsymbol{\Lambda}_{\text{P},m}^{1/2} \mathbf{q}_k \\ &\approx \sigma_x^2 \frac{\text{tr}\left\{\boldsymbol{\Lambda}_{\text{P},m}\boldsymbol{\Lambda}^{-1}\right\}}{\text{tr}\left\{\boldsymbol{\Lambda}_{\text{P},m}\right\}} \\ &= \sigma_x^2 \frac{\text{tr}\left\{\boldsymbol{\Lambda}_{\text{D},m}^{-2}\right\} + NM - m}{\text{tr}\left\{\boldsymbol{\Lambda}_{\text{P},m}\right\}} \end{aligned} \tag{66}$$

and the noise power is

$$\begin{aligned} N_{\text{o,SWF-DF}} &= \sigma_u^2 \mathbf{w}_{\text{SWF-DF},k}^{\text{H}} \mathbf{w}_{\text{SWF-DF},k} \\ &= \sigma_u^2 \beta_{\text{SWF},m} \mathbf{q}_k^{\text{H}} \boldsymbol{\Lambda}_{\text{P},m}^{1/2} \boldsymbol{\Lambda}^{-1} \mathbf{V}^{\text{H}} \mathbf{V} \boldsymbol{\Lambda}^{-1} \boldsymbol{\Lambda}_{\text{P},m}^{1/2} \mathbf{q}_k \\ &\approx \sigma_u^2 \frac{\text{tr}\left\{\boldsymbol{\Lambda}_{\text{P},m}\boldsymbol{\Lambda}^{-2}\right\}}{\text{tr}\left\{\boldsymbol{\Lambda}_{\text{P},m}\right\}}. \end{aligned} \tag{67}$$

The SINR after processing the SWF symbol by the DF of (64) is found by combining (65)–(67) to be

$$\text{SINR}_{\text{o,SWF-DF}}(m) = \frac{|\alpha|^2 \left(\text{tr}\left\{\boldsymbol{\Lambda}_{\text{D}}^{-2}\right\} + NM - m\right)^2}{\text{tr}\left\{\boldsymbol{\Lambda}_{\text{P},m}\right\}\left(\sigma_x^2\left(\text{tr}\left\{\boldsymbol{\Lambda}_{\text{D},m}^{-2}\right\} + NM - m\right) + \sigma_u^2 \text{tr}\left\{\boldsymbol{\Lambda}_{\text{P},m}\Lambda^{-2}\right\}\right)}, \tag{68}$$

so the resultant processing gain is

$$\Delta_{\text{SWF-DF}}(m) = \frac{NM\left(\sigma_x^2 + \sigma_u^2\right)\left(\text{tr}\left\{\boldsymbol{\Lambda}_{\text{D}}^{-2}\right\} + NM - m\right)^2}{\text{tr}\left\{\boldsymbol{\Lambda}_{\text{P},m}\right\}\left(\sigma_x^2\left(\text{tr}\left\{\boldsymbol{\Lambda}_{\text{D},m}^{-2}\right\} + NM - m\right) + \sigma_u^2 \text{tr}\left\{\boldsymbol{\Lambda}_{\text{P},m}\boldsymbol{\Lambda}^{-2}\right\}\right)}. \tag{69}$$

The LDF structure of (32), when applied to the SWF symbol of (18), takes the form

$$\begin{aligned} \mathbf{w}_{\text{SWF-LDF},k} &= \mathbf{V}\tilde{\boldsymbol{\Lambda}}^{-1}\mathbf{V}^{\text{H}} \left(\beta_{\text{SWF},m}^{1/2} \mathbf{V}\boldsymbol{\Lambda}_{\text{P},m}^{1/2} \mathbf{q}_k\right). \\ &= \beta_{\text{SWF},m}^{1/2} \mathbf{V}\tilde{\boldsymbol{\Lambda}}^{-1}\boldsymbol{\Lambda}_{\text{P},m}^{1/2} \mathbf{q}_k \end{aligned} \tag{70}$$

The derivation of the SINR after processing with the LDF of (70) closely follows the steps taken in (65)–(67), resulting in an output SINR of

$$\begin{aligned} &\text{SINR}_{\text{o,SWF-LDF}}(m) \\ &= \frac{|\alpha|^2 \left(\text{tr}\left\{\boldsymbol{\Lambda}_{\text{P},m}\tilde{\boldsymbol{\Lambda}}^{-1}\right\}\right)^2}{\text{tr}\left\{\boldsymbol{\Lambda}_{\text{P},m}\right\}\left(\sigma_x^2 \text{tr}\left\{\boldsymbol{\Lambda}_{\text{P},m}\tilde{\boldsymbol{\Lambda}}^{-2}\boldsymbol{\Lambda}\right\} + \sigma_u^2 \text{tr}\left\{\boldsymbol{\Lambda}_{\text{P},m}\tilde{\boldsymbol{\Lambda}}^{-2}\right\}\right)}, \end{aligned} \tag{71}$$

which yields a processing gain of

$$\begin{aligned} &\Delta_{\text{SWF-LDF}}(m) \\ &= \frac{NM\left(\sigma_x^2 + \sigma_u^2\right)\left(\text{tr}\left\{\boldsymbol{\Lambda}_{\text{P},m}\tilde{\boldsymbol{\Lambda}}^{-1}\right\}\right)^2}{\text{tr}\left\{\boldsymbol{\Lambda}_{\text{P},m}\right\}\left(\sigma_x^2 \text{tr}\left\{\boldsymbol{\Lambda}_{\text{P},m}\tilde{\boldsymbol{\Lambda}}^{-2}\boldsymbol{\Lambda}\right\} + \sigma_u^2 \text{tr}\left\{\boldsymbol{\Lambda}_{\text{P},m}\tilde{\boldsymbol{\Lambda}}^{-2}\right\}\right)}. \end{aligned} \tag{72}$$

### C. Processing Gain of SDP Symbols

The final symbol-design method under consideration is the SDP method given in (13). When an MF is used, the scaling factor of (14) again causes the signal power after processing to reduce to

$$S_{\text{o,SDP-MF}} = |\alpha|^2 \left|\mathbf{w}_{\text{SDP-MF},k}^{\text{H}} \mathbf{c}_{\text{SDP},k}\right|^2 = |\alpha|^2 \tag{73}$$

and the noise power from (42) to become

$$N_{\text{o,SDP-MF}} = \sigma_u^2 \mathbf{w}_{\text{SDP-MF},k}^{\text{H}} \mathbf{w}_{\text{SDP-MF},k} = \sigma_u^2. \tag{74}$$

The clutter power after filtering with the MF of (13) is then found from (41) to be

$$\begin{aligned} R_{\mathrm{o,SDP-MF}} &= \sigma_x^2 \mathbf{w}_{\mathrm{SDP-MF},k}^{\mathrm{H}} \mathbf{V}\boldsymbol{\Lambda}\mathbf{V}^{\mathrm{H}} \mathbf{w}_{\mathrm{SDP-MF},k} \\ &= \sigma_x^2 \beta_{\mathrm{SDP},m} \mathbf{q}_{\mathrm{ND},k}^{\mathrm{H}} \boldsymbol{\Lambda}_{\mathrm{ND},m}^2 \mathbf{q}_{\mathrm{ND},k} \\ &\approx \sigma_x^2 \frac{\mathrm{tr}\left\{\boldsymbol{\Lambda}_{\mathrm{ND},m}^2\right\}}{\mathrm{tr}\left\{\boldsymbol{\Lambda}_{\mathrm{ND},m}\right\}}, \end{aligned} \tag{75}$$

yielding an expected output SINR of

$$\mathrm{SINR}_{\mathrm{o,SDP-MF}}(m) = \frac{|\alpha|^2}{\sigma_x^2 \frac{\mathrm{tr}\left\{\boldsymbol{\Lambda}_{\mathrm{ND},m}^2\right\}}{\mathrm{tr}\left\{\boldsymbol{\Lambda}_{\mathrm{ND},m}\right\}} + \sigma_u^2}. \tag{76}$$

From (76), the MF produces a processing gain for the SDP symbol of

$$\Delta_{\mathrm{SDP},MF}(m) = \frac{NM\left(\sigma_x^2 + \sigma_u^2\right)}{\sigma_x^2 \frac{\mathrm{tr}\left\{\boldsymbol{\Lambda}_{\mathrm{ND},m}^2\right\}}{\mathrm{tr}\left\{\boldsymbol{\Lambda}_{\mathrm{ND},m}\right\}} + \sigma_u^2}. \tag{77}$$

The DF associated with the SDP symbol is found by substituting (13) into (31):

$$\begin{aligned} \mathbf{w}_{\mathrm{SDP-DF},k} &= \mathbf{V}\boldsymbol{\Lambda}^{-1}\mathbf{V}^{\mathrm{H}}\left(\beta_{\mathrm{SDP},m}^{1/2}\mathbf{V}_{\mathrm{ND},m}\boldsymbol{\Lambda}_{\mathrm{ND},m}^{1/2}\mathbf{q}_{\mathrm{ND},k}\right) \\ &= \beta_{\mathrm{SDP},m}^{1/2}\mathbf{V}\begin{bmatrix}\mathbf{0}_{m\times(NM-m)} \\ \boldsymbol{\Lambda}_{\mathrm{ND}}^{-1/2}\end{bmatrix}\mathbf{q}_{\mathrm{ND},k}. \end{aligned} \tag{78}$$

Using (13) and (78), the signal power after the DF is

$$\begin{aligned} S_{\mathrm{o,SDP-DF}} &= |\alpha|^2\left|\mathbf{w}_{\mathrm{SDP-DF},k}^{\mathrm{H}}\mathbf{c}_{\mathrm{SDP},k}\right|^2 \\ &= |\alpha|^2\left|\beta_{\mathrm{SDP},m}\mathbf{q}_{\mathrm{ND},k}^{\mathrm{H}}\mathrm{tr}\left\{\boldsymbol{\Lambda}_{\mathrm{ND},m}^{-1/2}\boldsymbol{\Lambda}_{\mathrm{ND},m}^{1/2}\right\}\mathbf{q}_{\mathrm{ND},k}\right|^2 \\ &\approx \frac{|\alpha|^2\beta_{\mathrm{SDP},m}^2(NM-m)^2}{(NM)^2} \\ &= \frac{|\alpha|^2(NM-m)^2}{\left(\mathrm{tr}\left\{\boldsymbol{\Lambda}_{\mathrm{ND},m}\right\}\right)^2}. \end{aligned} \tag{79}$$

Applying (78) to (41) reveals that the interference power after the DF is

$$\begin{aligned} R_{\mathrm{o,SDP-DF}} &= \sigma_x^2 \mathbf{w}_{\mathrm{SDP-DF},k}^{\mathrm{H}}\mathbf{V}\boldsymbol{\Lambda}\mathbf{V}^{\mathrm{H}}\mathbf{w}_{\mathrm{SDP-DF},k} \\ &= \sigma_x^2\beta_{\mathrm{SDP},m}\mathbf{q}_{\mathrm{ND},k}^{\mathrm{H}}\left[\mathbf{0}\,\middle|\,\boldsymbol{\Lambda}_{\mathrm{ND}}^{-1/2}\right]\boldsymbol{\Lambda}\begin{bmatrix}0 \\ \boldsymbol{\Lambda}_{\mathrm{ND}}^{-1/2}\end{bmatrix}\mathbf{q}_{\mathrm{ND},k} \\ &= \sigma_x^2\frac{(NM-m)}{\mathrm{tr}\left\{\boldsymbol{\Lambda}_{\mathrm{ND},m}\right\}}. \end{aligned} \tag{80}$$

Similarly, the noise power after the DF of (78) is found from (42) to be

$$\begin{aligned} &N_{\mathrm{o,SDP-DF}} \\ &\quad= \sigma_u^2\mathbf{w}_{\mathrm{SDP-DF},k}^{\mathrm{H}}\mathbf{w}_{\mathrm{SDP-DF},k} \\ &\quad= \sigma_u^2\beta_{\mathrm{SDP},m}\mathbf{q}_{\mathrm{ND},k}^{\mathrm{H}}\left[\mathbf{0}\,\middle|\,\boldsymbol{\Lambda}_{\mathrm{ND}}^{-1/2}\right]\mathbf{V}^{\mathrm{H}}\mathbf{V}\begin{bmatrix}0 \\ \boldsymbol{\Lambda}_{\mathrm{ND}}^{-1/2}\end{bmatrix}\mathbf{q}_{\mathrm{ND},k} \\ &\quad= \sigma_u^2\frac{\mathrm{tr}\left\{\boldsymbol{\Lambda}_{\mathrm{ND},m}^{-1}\right\}}{\mathrm{tr}\left\{\boldsymbol{\Lambda}_{\mathrm{ND},m}\right\}}. \end{aligned} \tag{81}$$

Therefore, the output SINR for SDP using the DF is found from (79)–(81) to be

$$\begin{aligned} &\mathrm{SINR}_{\mathrm{o,SDP-DF}}(m) \\ &\quad= \frac{|\alpha|^2(NM-m)^2}{\mathrm{tr}\left\{\boldsymbol{\Lambda}_{\mathrm{ND},m}\right\}\left(\sigma_x^2(NM-m)+\sigma_u^2\mathrm{tr}\left\{\boldsymbol{\Lambda}_{\mathrm{ND},m}^{-1}\right\}\right)}. \end{aligned} \tag{82}$$

The processing gain obtained by the DF of (78) is then found from (82) and (38) to be

$$\begin{aligned} &\Delta_{\mathrm{SDP-DF}}(m) \\ &\quad= \frac{NM\left(\sigma_x^2+\sigma_u^2\right)(NM-m)^2}{\mathrm{tr}\left\{\boldsymbol{\Lambda}_{\mathrm{ND},m}\right\}\left(\sigma_x^2(NM-m)+\sigma_u^2\mathrm{tr}\left\{\boldsymbol{\Lambda}_{\mathrm{ND},m}^{-1}\right\}\right)}. \end{aligned} \tag{83}$$

The final design under consideration is an SDP symbol filtered with the LDF structure of (32). From (13) and (32), this filter takes the form

$$\begin{aligned} \mathbf{w}_{\mathrm{SDP-LDF},k} &= \mathbf{V}\tilde{\boldsymbol{\Lambda}}^{-1}\mathbf{V}^{\mathrm{H}}\left(\beta_{\mathrm{SDP},m}^{1/2}\mathbf{V}_{\mathrm{ND},m}\boldsymbol{\Lambda}_{\mathrm{ND},m}^{1/2}\mathbf{q}_{\mathrm{ND},k}\right) \\ &= \beta_{\mathrm{SDP},m}^{1/2}\mathbf{V}\begin{bmatrix}\mathbf{0}_{m\times(NM-m)} \\ \tilde{\boldsymbol{\Lambda}}_{\mathrm{ND},m}^{-1}\end{bmatrix}\boldsymbol{\Lambda}_{\mathrm{ND},m}^{1/2}\mathbf{q}_{\mathrm{ND},k}, \end{aligned} \tag{84}$$

Filtering the SDP symbol of (13) with the LDF of (84) results in an average output signal power of

$$\begin{aligned} S_{\mathrm{o,SDP-LDF}} &= |\alpha|^2\left|\mathbf{w}_{\mathrm{SDP-LDF},k}^{\mathrm{H}}\mathbf{c}_{\mathrm{SDP},k}\right|^2 \\ &= |\alpha|^2\left|\beta_{\mathrm{SDP},m}\mathbf{q}_{\mathrm{ND},k}^{\mathrm{H}}\boldsymbol{\Lambda}_{\mathrm{ND},m}^{1/2}\tilde{\boldsymbol{\Lambda}}_{\mathrm{ND},m}^{-1}\boldsymbol{\Lambda}_{\mathrm{ND},m}^{1/2}\mathbf{q}_{\mathrm{ND},k}\right|^2 \\ &\approx \frac{|\alpha|^2\left(\mathrm{tr}\left\{\boldsymbol{\Lambda}_{\mathrm{ND},m}\tilde{\boldsymbol{\Lambda}}_{\mathrm{ND},m}^{-1}\right\}\right)^2}{\left(\mathrm{tr}\left\{\boldsymbol{\Lambda}_{\mathrm{ND},m}\right\}\right)^2}. \end{aligned} \tag{85}$$

The clutter power after filtering with (84) is found from (41) to be

$$\begin{aligned} R_{\mathrm{o,SDP-LDF}} &= \sigma_x^2\mathbf{w}_{\mathrm{SDP-LDF},k}^{\mathrm{H}}\mathbf{V}\boldsymbol{\Lambda}\mathbf{V}^{\mathrm{H}}\mathbf{w}_{\mathrm{SDP-LDF},k} \\ &= \sigma_x^2\frac{\mathrm{tr}\left\{\boldsymbol{\Lambda}_{\mathrm{ND},m}^2\tilde{\boldsymbol{\Lambda}}_{\mathrm{ND},m}^{-2}\right\}}{\mathrm{tr}\left\{\boldsymbol{\Lambda}_{\mathrm{ND},m}\right\}}. \end{aligned} \tag{86}$$

The noise power is then similarly found from (84) and (42):

$$\begin{aligned} N_{\mathrm{o,SDP-LDF}} &= \sigma_x^2\mathbf{w}_{\mathrm{SDP-LDF},k}^{\mathrm{H}}\mathbf{w}_{\mathrm{SDP-LDF},k} \\ &= \sigma_u^2\frac{\mathrm{tr}\left\{\boldsymbol{\Lambda}_{\mathrm{ND},m}\tilde{\boldsymbol{\Lambda}}_{\mathrm{ND},m}^{-2}\right\}}{\mathrm{tr}\left\{\boldsymbol{\Lambda}_{\mathrm{ND},m}\right\}}. \end{aligned} \tag{87}$$

Equations (85)–(87) are then combined to find that the output SINR from LDF filtering of the SDP symbol is

$$\begin{aligned} &\mathrm{SINR}_{\mathrm{o,SDP-LDF}}(m) = \\ &\quad\frac{|\alpha|^2\left(\mathrm{tr}\left\{\boldsymbol{\Lambda}_{\mathrm{ND},m}\tilde{\boldsymbol{\Lambda}}_{\mathrm{ND},m}^{-1}\right\}\right)^2}{\mathrm{tr}\left\{\boldsymbol{\Lambda}_{\mathrm{ND},m}\right\}\left(\sigma_x^2\mathrm{tr}\left\{\boldsymbol{\Lambda}_{\mathrm{ND},m}^2\tilde{\boldsymbol{\Lambda}}_{\mathrm{ND},m}^{-2}\right\}+\sigma_u^2\mathrm{tr}\left\{\boldsymbol{\Lambda}_{\mathrm{ND},m}\tilde{\boldsymbol{\Lambda}}_{\mathrm{ND},m}^{-2}\right\}\right)}, \end{aligned} \tag{88}$$

resulting in a processing gain of

$$\Delta_{\mathrm{SDP-LDF}}(m) = \frac{NM\left(\sigma_x^2+\sigma_u^2\right)\left(\mathrm{tr}\left\{\boldsymbol{\Lambda}_{\mathrm{ND},m}\tilde{\boldsymbol{\Lambda}}_{\mathrm{ND},m}^{-1}\right\}\right)^2}{\mathrm{tr}\left\{\boldsymbol{\Lambda}_{\mathrm{ND},m}\right\}\left(\sigma_x^2\mathrm{tr}\left\{\boldsymbol{\Lambda}_{\mathrm{ND},m}^2\tilde{\boldsymbol{\Lambda}}_{\mathrm{ND},m}^{-2}\right\}+\sigma_u^2\mathrm{tr}\left\{\boldsymbol{\Lambda}_{\mathrm{ND},m}\tilde{\boldsymbol{\Lambda}}_{\mathrm{ND},m}^{-2}\right\}\right)}. \quad (89)$$

REFERENCES


[1] Winkler, V., Detlefsen, J., Siart, U., Buchler, J., and Wagner, M.
Automotive radar sensor with communication capability.
In *7th European Conference on Wireless Technology*, Amsterdam, the Netherlands, Oct. 2004, 305–308.

[2] Winkler, V., and Detlefsen, J.
Automotive 24 GHz pulse radar extended by a DQPSK communication channel.
In *European Radar Conference, 2007*, Munich, Germany, Oct. 2007, 138–141.

[3] Bocquet, M., Loyez, C., Lethien, C., Deparis, N., Heddebaut, M., Rivenq, A., and Rolland, N.
A multifunctional 60-GHz system for automotive applications with communication and positioning abilities based on time reversal.
In *2010 European Radar Conference*, Paris, France, Sept.–Oct. 2010, 61–64.

[4] Reichardt, L., Sturm, C., Grunhaupt, F., and Zwick, T.
Demonstrating the use of the IEEE 802.11P Car-to-Car communication standard for automotive radar.
In *6th European Conference on Antennas and Propagation*, Prague, Czech Republic, Mar. 2012, 1576–1580.

[5] Chapin, J.
Shared spectrum access for radar and communications (SSPARC).
[Online]. Available: http://www.darpa.mil/program/shared-spectrum-access-for-radar-and-communications.

[6] Blunt, S. D., and Yatham, P.
Waveform design for radar-embedded communications.
In *International Waveform Diversity and Design Conference*, Pisa, Italy, June 2007, 214–218.

[7] Blunt, S. D., Yatham, P., and Stiles, J.
Intrapulse radar-embedded communications.
*IEEE Transactions on Aerospace and Electronic Systems*, **46**, 3 (Jul. 2010), 1185–1200.

[8] Metcalf, J., Blunt, S., and Perrins, E.
Detector design and intercept metrics for intra-pulse radar-embedded communications.
In *Military Communications Conference*, Baltimore, MD, Nov. 2011, 188–192.

[9] Blunt, S. D., Metcalf, J. G., Biggs, C. R., and Perrins, E.
Performance characteristics and metrics for intra-pulse radar-embedded communications.
*IEEE Journal on Selected Areas in Communications*, **29**, 10 (Dec. 2011), 2057–2066.

[10] Scholtz, R. A.
The origins of spread-spectrum communications.
*IEEE Transactions on Communications*, **30**, 5 (May 1982), 822–854.

[11] Gevargiz, J., Das, P. K., and Milstein, L. B.
Adaptive narrow-band interference rejection in a DS spread-spectrum intercept receiver using transform domain signal processing techniques.
*IEEE Transactions on Communications*, **37**, 12 (Dec. 1989), 1359–1366.

[12] Fancey, C., and Alabaster, C. M.
The metrication of low probability of intercept waveforms.
In *2010 International Waveform Diversity and Design Conference*, Niagara Falls, Canada, Aug. 2010, 58–62.

[13] Proakis, J. G., and Salehi, M.
*Digital Communications* (5th ed.). New York: McGraw-Hill, 2007.

[14] Lewis, B. L., and Kretschmer, F. F.
Linear frequency modulation derived polyphase pulse compression codes.
*IEEE Transactions on Aerospace and Electronic Systems*, **AES-18**, 5 (Sept. 1982), 637–641.

[15] Kay, S. M.
*Fundamentals of Statistical Signal Processing*. Vol. 2: *Detection Theory*. Upper Saddle River, NJ: Prentice Hall, 1998.

[16] Sijbers, J., den Dekker, A. J., Raman, E., and Van Dyck, D.
Parameter estimation from magnitude MR images.
*International Journal of Imaging Systems and Technology*, **10**, 2 (1999), 109–114.

[17] Verdu, S.
*Multiuser Detection*. New York: Cambridge University Press, 1998.

[18] Lupas, R., and Verdu, S.
Linear multiuser detectors for synchronous code-division multiple-access channels.
*IEEE Transactions on Information Theory*, **35**, 1 (Jan. 1989), 123–136.


**Justin Metcalf** (S'08) received a bachelor's degree in computer engineering from Kansas State University in 2006. From 2006 to 2008 he was at the Flight Simulation Labs of Lockheed Martin Aeronautics in Fort Worth, TX. From 2008 to 2014 he was with the Radar Systems & Remote Sensing Lab of the University of Kansas, where he obtained a master's degree (with honors) in electrical engineering in 2011 and a Ph.D. degree (with honors) in electrical engineering in 2015. He was the recipient of the Richard and Wilma Moore Award for the best departmental master's thesis in 2011–2012. In 2014 he joined the sensors directorate of the Air Force Research Laboratory as a research electronics engineer.

**Cenk Sahin** (S'06) received a B.S. degree (summa cum laude) in electrical and computer engineering from the University of Missouri–Kansas City in 2008 and an M.S. degree (with honors) in electrical engineering from the University of Kansas, Lawrence, in 2012. Currently, he is a Ph.D. degree candidate in electrical engineering at the University of Kansas. His general research interests include digital communication theory, information theory, queueing theory, and their application to wireless communication systems.

**Shannon D. Blunt** (S'96—M'02—SM'07) received a Ph.D. degree in electrical engineering from the University of Missouri in 2002. From 2002 to 2005 he was with the radar division of the Naval Research Laboratory in Washington, DC. Since 2005 he has been with the department of electrical engineering and computer science at the University of Kansas, where he is currently a professor and the director of the Radar Systems & Remote Sensing Lab (RSL).

In 2012 Prof. Blunt received the IEEE/AESS Nathanson Memorial Radar Award, and in 2008 he received the AFOSR Young Investigator Award. He has over 100 refereed journal and conference publications, 11 patents, and five book chapters, and coedited the book *Principles of Waveform Diversity and Design*.

He is a member of the IEEE/AESS radar systems panel, where he is currently the chair of the conferences committee. He is an associate editor for *IEEE Transactions on Aerospace and Electronic Systems* and is on the editorial board for *IET Radar, Sonar & Navigation*. He was the general chair of the 2011 IEEE Radar Conference in Kansas City and is a member of the program committee for the MSS Tri-Service Radar Symposium series. He was the chair of the NATO SET-179 research task group on Dynamic Waveform Diversity & Design and a member of SET-182 on Radar Spectrum Engineering & Management and SET-227 on Cognitive Radar. He is a senior member of IEEE.

**Muralidhar Rangaswamy** (S'89—M'93—SM'98—F'06) received a B.E. degree in electronics engineering from Bangalore University, Bangalore, India, in 1985 and M.S. and Ph.D. degrees in electrical engineering from Syracuse University, Syracuse, NY, in 1992. He is presently employed as the senior advisor for radar research at the RF Exploitation Branch within the sensors directorate of the Air Force Research Laboratory (AFRL). Prior to this he has held industrial and academic appointments.

His research interests include radar signal processing, spectrum estimation, modeling non-Gaussian interference phenomena, and statistical communication theory. He has coauthored more than 200 refereed journal and conference-record papers in the areas of his research interests. Additionally, he is a contributor to eight books and a coinventor on three U.S. patents.

Dr. Rangaswamy is the technical editor (associate editor-in-chief) for radar systems of *IEEE Transactions on Aerospace and Electronic Systems*. He served as the co-editor-in-chief for the journal *Digital Signal Processing* between 2005 and 2011 and on the senior editorial board of the *IEEE Journal of Selected Topics in Signal Processing* from January 2012 to December 2014. He was a two-term elected member of the sensor array and multichannel processing technical committee of the IEEE Signal Processing Society between January 2005 and December 2010 and serves as a member of the radar systems panel in the IEEE-AES Society. He was the general chairman for the 4th IEEE Workshop on Sensor Array and Multichannel Processing, Waltham, MA, in July 2006. He has served on the technical committee of the IEEE Radar Conference series in a myriad of roles (track chair, session chair, special session organizer and chair, paper selection committee member, tutorial lecturer). He served as the publicity chair for the First IEEE International Conference on Waveform Diversity and Design, Edinburgh, United Kingdom, in November 2004. He presently serves on the conference subcommittee of the RSP. He was the technical program chairman for the 2014 IEEE Radar Conference.

Dr. Rangaswamy received the IEEE Warren White Radar Award in 2013, the 2013 Affiliate Societies Council Dayton Outstanding Scientist and Engineer Award, the 2007 IEEE Region 1 Award, the 2006 IEEE Boston Section Distinguished Member Award, and the 2005 IEEE-AESS Fred Nathanson memorial outstanding young radar engineer award. He was elected as a fellow of the IEEE in January 2006 with the citation "for contributions to mathematical techniques for radar space-time adaptive processing." He received the 2012 and 2005 Charles Ryan basic research award from the sensors directorate of AFRL, in addition to more than 40 scientific achievement awards.